TR
Technical Report

Technical Report

Pre-study 5.2

ESA's multi-level global thermosphere data products consistent with Swarm and GRACE(-FO)

Professor Ehsan Forootan

2023

Working Title:
Pre-study 5.2 for the ESA's multi-level global thermosphere data products consistent with Swarm and GRACE(-FO)

Geodesy Group, Department of Planning, Aalborg University

Professor Ehsan Forootan
Rendsburggade 14,
9000 Aalborg, Denmark
efo@plan.aau.dk

Swarm DISC

Summary

This technical reports is prepared for the Swarm DISC programme to assess the possibility of using the space-based along track Thermospheric Neutral Density (TND) estimates for generating global multi-level TND data products (i.e., a new level 3, L3, TND product). For this, the TND estimates along the CHAMP, GRACE, and Swarm satellites are used as observation within the sequential Calibration and Data Assimilation (C/DA) framework proposed by Forootan et al. 2020 and 2022 [10, 12].

The C/DA approach is applied to re-calibrate four key parameters of the NRLMSISE-00 model, which are most sensitive to the thermospheric neutral mass and thermospheric temperature. The model with re-calibrated parameters is called 'C/DA-NRLMSISE-00', whose outputs fit to the space-based TNDs. The C/DA-NRLMSISE-00 is able to forecast TNDs and individual neutral mass compositions at any predefined vertical level (i.e., the same vertical coverage as the NRLMSISE-00) and arbitrary spatial-temporal resolution. Therefore, the C/DA method is tested to produce level 3 (L3) TND data consistent with space-based TND estimates.

Seven periods (October 2003, July 2004, March 2008, April 2010, March 2015, September 2017, and September 2020), associated with relatively high geomagnetic activity, are selected for our investigations because most of available models represent difficulties to provide reasonable TND estimations. Independent comparisons (validations) are performed with the space-based TNDs that were not used within the C/DA framework, as well as with the outputs of other thermosphere models such as the Jacchia-Bowman 2008 (JB08) and the High Accuracy Satellite Drag Model (HASDM). The numerical results indicate an average 52%, 50%, 56%, 25%, 47%, 54%, and 63% improvement in the Root Mean Squared Errors (RMSE) of the C/DA-NRLMSISE00's TND forecasts compared to the along track TND estimates of GRACE (2003, average altitude 490 km), GRACE (2004, average altitude 486 km), CHAMP (2008, average altitude 343 km), GOCE (2010, average altitude 270 km), Swarm-B (2015, average altitude 520 km), Swarm-B (2017, average altitude 514 km), and Swarm-B (2020, average altitude 512 km), respectively.

The choice of spatial (horizontal and vertical) and temporal sampling for producing the L3 data is investigated by implementing empirical covariance matrices. The results indicate that the global L3 fields can be produced hourly with 5 degree horizontal and 25 km vertical resolution to provide the same sampling characteristics that one could expect from NRLMSISE-00. Justification of the reasonable vertical range for the L3 products is found to be difficult because the validation data only

covered the altitude of $\sim$ 250-550 km.

Nevertheless, our global assessments indicate that the C/DA approach is able to extrapolate the impact of the space-based TND estimates globally, even though the observations are along track and correspond to a limited range of altitude coverage. The magnitude of the differences between empirical models and the L3 TND data is found to be considerable for geodetic and orbit determination applications. Thus, we recommend the application of C/DA and a consistently processed space-based along track TND data for generating the ESA's L3 TND products. The global and along track TND data sets during the seven storm periods of this study are submitted along with this report to the Swarm DISC team. For queries, please contact Ehsan Forootan [1].

[1] efo@plan.aau.dk

Acknowledgements

This study is led by Ehsan Forootan from the geodesy Group at Aalborg University, Denmark. We would like to thank Ms Mona Kosary (University of Tehran) for supporting the computational activities. The technical supports are provided by Claudia Borries and Timothy Kodikara (German Aerospace Center, DLR, Neustrelitz, Germany), Eelco Doornbos (KNMI: De Bilt, Utrecht, Netherlands), Christian Siemes (Delft University of Technology, Netherlands), and Saeed Farzaneh (University of Tehran). The author would like to acknowledge the support by the ESA Swarm DISC (ESA Contract No. 4000109587/13/I-NB). For details, contact Ehsan Forootan `efo@plan.aau.dk`, last update on 01.2023.

Contents

List of Figures

CHAPTER 1

Introduction

Space weather describes physical processes caused by the Sun's radiation of energy including the variations of the Earth's magnetic field, and changes in the states of the upper atmosphere – between the altitude of around 100 km up to 2000 km – comprising both the thermosphere and the ionosphere. As a result, the upper atmosphere region exhibits a dynamically coupled non-linear system of chemical and physical processes.

An accurate estimation of Thermospheric Neutral Density (TND) is important for designing the Low-Earth-Orbit (LEO) missions mainly those with the altitude of less than 1000 km. It is also essential, for example, to predict satellite missions' life time, planning their required on-board fuel, performing reliable attitude control, designing orbital manoeuvre, as well as predicting and performing Earth re-entry (see discussions in e.g., [4, 39, 15]).

Predicting the thermosphere-ionosphere system is challenging because it is highly influenced by the solar irradiance, and it depends on the state of the neutral temperature and composition. External forces such as those related to the space weather events (e.g., [35, 29, 28]), as well as interactions between neutral molecules with charged particles considerably influence the thermopsheric variability ([34]). Empirical thermosphere or coupled thermosphere-ionosphere models are common tools to provide an estimation of TND (e.g., for drag computations), however, their accuracy is limited due to simplification of model structure, coarse sampling of model inputs, and the model's dependencies on the calibration period.

Satellite geodetic missions such as the Challenging Minisatellite Payload (CHAMP, 2000-2010, [30]), the Gravity Recovery and Climate Experiment (GRACE, 2002-2017, [38]) and its Follow-On mission (GRACE-FO, launched in 2018, [8]), Gravity field and steady-state Ocean Circulation Explorer (GOCE, 2009-2013, [1]), and the European Space Agency (ESA)'s Swarm mission (Swarm-A, -B, and -C launched in 2013, [41]) are equipped with accelerometer sensor to measure non-gravitational forces acting on their surface. The dominant portion of these forces is due to the atmospheric drag, which can be used to estimate TNDs along track of satellites with very high temporal rates (e.g., [37, 22, 40]). In the recent past, great attempts have been taken to produce these estimates from space missions such as CHAMP, GRACE, GOCE, GRACE-FO, and Swarm on-board accelerometer measurements (or from dynamic their orbits).

Various data providers, e.g., the European Space Agency (ESA, `https://earth.esa.int`, and research centers (e.g., [22], `ftp://thermosphere.tudelft.nl/`, and

[40]) freely share their TND estimates. However, these measurements are only available along the orbits of these space missions. Therefore, their usage is limited for applications such as orbit prediction, or the global assessment of the upper atmosphere.

A logical step to make the best use of space-based TND observations and available models can be realised through the mathematical merging frameworks that build a connection between them. For example, (1) correction fields are applied as a ratio of TNDs from LEO satellites and those of models ([5, 6, 24, 33, 31, 11, 42]). However, this method can only be used for reanalyzing and now-casting the thermosphere, and the reliability of these ratio fields, derived by a limited number of satellite tracks, might be treated with caution. (2) Statistical decomposition techniques ([9]) have been used to extract the dominant structures of the upper atmosphere dynamics. Then, in the prediction step, state-space techniques such as the Kalman Filter (KF, [14]) are applied to forecast thermosphere variations. Previous studies (e.g., [19, 18, 17, 20, 21]) successfully applied this approach during geomagnetic storms because the pronounced temporal and spatial changes during these events enhance the model-data integration. This technique might be less efficient during calm periods, where the level of uncertainties of models and data is comparable. (3) Sequential Data Assimilation (DA) techniques are found to be efficient for merging observations and model outputs, while decreasing the model uncertainties (e.g., [16, 13, 23, 26, 3]). However, the DA techniques mostly focus on updating the model states and they are not very efficient to extend the along track measurements to cover the whole globe. Besides, they are not very efficient for forecasting. (4) The Calibration and Data Assimilation (C/DA) provides the opportunity to update the model's states (similar to DA) but its advantage is that key model parameters can also be simultaneously calibrated (e.g., [10]). The calibrated parameters then can be used to simulate TNDs globally (i.e., now-cast them globally), or to forecast them in future.

The C/DA methodology was recently applied in (e.g., [12]) to re-calibrate the commonly used NRLMSISE-00 empirical thermosphere model ([25]) against TND estimated of GRACE (at the altitude of $\sim$ 410 km during February 2015). The resulting re-calibrated model, known as 'C/DA-NRLMSISE-00', was then used for now-casting TNDs and individual neutral mass compositions for 3 hours, as well as for forecasting the next 21 hours. The assessment was performed against TND estimations from the Precise Orbit Determination (POD) analysis of Swarm data at the altitude range of 470-520 km during February 2^{nd}-28^{th}, 2015. The geomagnetic index K_p and the solar activity index F_{107} of this period were varying between 2-5 and 110 - 150 sfu, respectively. Assessing the forecasts of TNDs with those along the Swarm-A ($\sim$ 467 km), Swarm-B ($\sim$ 521 km), and Swarm-C ($\sim$ 467 km) orbits showed that the Root Mean Squared Error (RMSE) was considerably reduced by 51, 57, and 54%, respectively. The authors also found a positive feedback of the new global multi-level TND fields for forecasting ionospheric variables such the electron density (Ne).

For the "Swarm DISC programme 2021's Open Call for Ideas for New data products, tools and services for Swarm", Forootan and co-authors proposed to leverage the

publicly available Swarm and GRACE(-FO) along track TND data, and producing the following level 3 (L3) TND data and modelling tools:

1- global TND data product, e.g., with 2.5 and 1 degree spatial resolution or in terms of spherical harmonics, e.g., up to degree and order 60, covering the altitudes of 350 km - 600 km;

2- calibration parameters to adjust the TND outputs of common empirical models, such as NRLMSISE-00, to simulate 3-dimensional (3D) TND values that are consistent with those of Swarm and GRACE(-FO); or alternatively, a new model that incorporates the calibrated parameters providing TNDs on any satellite tracks or globally on user-defined grids and altitudes.

Therefore, unlike other available global DA outputs, the proposed L3 TND data product (in 1) or the improved model (in 2) is based purely on openly available models and measurements, which makes it reproducible. Besides, the Swarm and GRACE(-FO) data provide high temporal resolution, as well as dense spatial resolution in the latitudinal (north/south) direction, which can be tested whether they result in producing more accurate global TND estimates.

In this report, we test the potential of the C/DA approach (in [10, 12]) to produce the "ESA's multi-level global thermosphere L3 data products consistent with Swarm and GRACE(-FO)". For this,

1- seven storm periods during 2003-2022 are defined to produce global multi-level TND fields, where the along track TND estimates of at least two satellite missions of CHAMP, GRACE, GOCE, and Swarm were available;

2- calibration windows of 1 to 22 hour are examined during the first test period, October 2003, to find a suitable integration setting;

3- horizontal and temporal sampling is studied to define reasonable resolution for producing the L3 TND data. This is done based on the inputs of our test period in October 2003, and estimating empirical covariance and correlation measures;

4- performing along track comparisons with models such as the High Accuracy Satellite Drag Model (HASDM, [36]), JB08 ([2]), and the original NRLMSISE00, as well as TNDs from CHAMP, GRACE, and Swarm during the selected seven storm periods;

5- performing a global assessment of spatial and temporal TND changes provided by the C/DA model during the seven periods. This is done by applying the the statistical method of Principal Component Analysis (PCA, [27]) to extract and compare dominant differences.

It is worth mentioning here that producing multi-level L3 TND products during calm periods is not included here, because, this is well covered by the relatively long-term assessment (in, e.g., [10, 12]).

CHAPTER 2

Method

2.1 Calibration and Data Assimilation (C/DA)

The Calibration and Data Assimilation (C/DA) technique (as in [32] and [10]) is a sequential approach that uses real-world observations (measurements) to update a model's states and simultaneously its selected model parameters. The C/DA approach is applied in this study to tune NRLMSISE-00 as basis (or background model) using space-based TND measurements such as those of CHAMP, GRACE(-FO), and Swarm. The implementation of C/DA is realised through a model-state equation, where the model derived TNDs and some model parameters are considered as unknowns of this system. A solution for this system is computed sequentially through minimizing the following cost function:

$$J(\mathbf{X}) = \frac{1}{2}[\mathbf{X} - \bar{\mathbf{X}}^b]^T(\mathbf{P}^b)^{-1}[\mathbf{X} - \bar{\mathbf{X}}^b] + \frac{1}{2}[\mathbf{H}\mathbf{X}^b - \mathbf{Y}]^T\mathbf{R}^{-1}(\mathbf{H}\mathbf{X}^b - \mathbf{Y}), \tag{2.1}$$

where $\mathbf{X}^b$ represents the ensemble of model parameters and model states, $\mathbf{P}^b$ and $\mathbf{H}$ are the error covariance matrix of the background model and the design matrix that relates TNDs to model states and parameters, respectively. The ensemble of TND measurements is represented by $\mathbf{Y}$, and $\mathbf{R}$ holds the uncertainty of these measurements. More details are provided in what follows.

To decide which model parameters must be updated (or calibrated) within the model-state equation (Eq. 2.1), we relied on our previous assessments (e.g., [10]), where the impact of the following input variables and parameters on the model derived TNDs were tested: altitude (H), geodetic latitude (φ) and longitude (λ), Local apparent Solar Time (LST), solar flux for previous day ($F10.7$) and its three-month average ($F10.7A$), 3-hourly magnetic index (Ap), as well as some model coefficients including: *pavgm*, *pd*, *pdl*, *pdm*, *pma*, *ps*, *pt*, *ptl*, *ptm* and *sam*. These coefficients are used to compute the number (or density) of He, O, N2, O2, Ar, H, and N, total mass density, as well as the neutral and exospheric temperature ([25]). In our previous study, we found that the first components of *ptm* and *pt* model coefficients, as well as the two constant biases that modify solar and geomagnetic indices (i.e., $dF10.7A = F10.7A - 150$ and $dAp = Ap - 4$) are the most sensitive parameters. Therefore, this study focuses on calibrating these four key parameters within the C/DA that uses space-based TND measurements as observation.

The core of C/DA is selected to be the Ensemble Kalman Filter (EnKF as in [7]). This technique uses the available measurements sequentially and based on their error covariances and those of model decides how to update model states and the selected parameters.

To formulate the C/DA, first, let us assume that the original NRLMSISE-00 model is mathematically represented as:

$$\text{Original model, i.e., NRLMSISE-00} : F(\Theta) = F(\Theta_P, \Theta_R, \Theta_I), \tag{2.2}$$

where Θ is a vector of parameters and input values in the model. In our formulation, we consider that Θ consists of $\Theta_{P_{m_1 \times 1}}$ that are the four key parameters ($m1 = 4$) to be updated through the C/DA, Θ_R represents those parameters that will remain unchanged during the calibration, and Θ_I indicates the input variables such as the solar and geomagnetic indices, location, and time.

Ensembles of the model's key parameters are generated by a Monte Carlo simulation that considers i^{th} (i.e., $i = 1, ...n$) ensemble members of the key parameters ($\mathbf{X}^b_{1,i}$) are expressed as:

$$\mathbf{X}^b_{1,i} = \Theta_P + \xi_i, \ i = 1, ...n, \tag{2.3}$$

where $\Theta_{P_{m_1 \times 1}}$ is a vector of default values of the key parameters in NRLMSISE-00 as in Eq. (2.2) plus random errors (ξ_i) that perturb these initial values. The noise magnitude is considered to be 10% of each variable. In the C/DA procedure, ensembles of 90 members ($n = 90$) are used to perform the numerical integration. Selection of the assimilation window is reported in Chapter 3, section 3.2.

The ensemble of key parameters ($\mathbf{X}^b_1$) and model states (i.e., simulated TNDs using perturbed key parameters ($\mathbf{X}^b_2$=$F(\Theta_P + \xi, \Theta_R, \Theta_I)$) are stored in the matrix $\mathbf{X}^b_{m \times n}$ as:

$$\mathbf{X}^b = \begin{bmatrix} \mathbf{X}^b_{1 m_1 \times n} \\ - - - - - \\ \mathbf{X}^b_{2 m_2 \times n} \end{bmatrix}, \tag{2.4}$$

where the upper-index 'b' represents the background model. The ensemble mean vector ($\bar{\mathbf{x}}^b_{m \times 1}$) of Eq. (2.4) and the covariance matrix of the background step ($\mathbf{P}^b_{m \times m}$) are defined as:

$$\bar{\mathbf{x}}^b = \begin{bmatrix} \bar{\mathbf{x}}^b_1 \\ \bar{\mathbf{x}}^b_2 \end{bmatrix}, (e.g., \ \bar{\mathbf{x}}^b_1 = \frac{1}{n} \sum_{i=1}^{n} \mathbf{x}^b_{1,i}), \tag{2.5}$$

$$\mathbf{P}^b = \frac{1}{n-1} (\mathbf{X}^b - \bar{\mathbf{x}}^b)(\mathbf{X}^b - \bar{\mathbf{x}}^b)^T. \tag{2.6}$$

In each analysis step, shown by the upper-index 'a', the estimation of key parameters and the model state ($\mathbf{X}^a$) follows:

$$\mathbf{X}^a_{m \times n} = \mathbf{X}^b + \mathbf{K}(\mathbf{Y} - \mathbf{H}\mathbf{X}^{\mathrm{b}}), \tag{2.7}$$

and their ensemble mean, shown by $\bar{\mathbf{x}}^a$, is computed as:

$$\bar{\mathbf{x}}^a_{m\times 1} = \bar{\mathbf{x}}^b + \mathbf{K}(\bar{\mathbf{y}} - \mathbf{H}\bar{\mathbf{x}}^b). \tag{2.8}$$

Here, $\mathrm{Y}_{m_2\times n}$ and $\bar{\mathbf{y}}_{m_2\times 1}$ represent the ensembles and the ensemble mean TND estimates from the C/DA, respectively. Therefore, according to Eqs. (2.7 and 2.8), the updates of key parameters and model states directly depend on the differences between the real observations (Y) and model predictions ($\mathbf{HX}^{\mathrm{b}}$), while considering their weights, which are reflected in the Kalman gain matrix ($\mathbf{K}_{\Theta m\times m_2}$) that is computed as:

$$\mathbf{K} = \mathbf{P}^{\mathrm{b}}\mathbf{H}^{\mathrm{T}}\left(\mathbf{H}\mathbf{P}^{\mathrm{b}}\mathbf{H}^{\mathrm{T}} + \mathbf{R}\right)^{-1}, \tag{2.9}$$

where $\mathbf{H}$ is the design matrix, which is defined as:

$$\mathbf{H}_{m_2\times m} = [\mathbf{0}_{m_2\times m_1} \;\; \mathbf{I}_{m_2\times m_2}]. \tag{2.10}$$

In Eq. (2.10), $\mathbf{0}_{m_2\times m_1}$ is a zero matrix, and $\mathbf{I}_{m_2\times m_2}$ represents the identity matrix. This means that in each step of the Kalman Filter process, the relationship between observations and model states is assumed to be linear.

The C/DA procedure (Eq. 2.4 to Eq. 2.10) has been evaluated at each time step to obtain the ensemble of parameters and states (i.e., $\mathbf{X}^a$), and their mean (i.e., $\bar{\mathbf{x}}^a$). Analogous to Eqs. (2.4 and 2.5), $\mathbf{X}^a$ and $\bar{\mathbf{x}}^a$ are divided into two section as:

$$\mathbf{X}^a = \begin{bmatrix} \mathbf{X}^a_{1\,m_1\times n} \\ ----- \\ \mathbf{X}^a_{2\,m_2\times n} \end{bmatrix}, \text{and} \qquad \mathbf{x}^a = \begin{bmatrix} \mathbf{x}^a_{1\,m_1\times n} \\ ----- \\ \mathbf{x}^a_{2\,m_2\times n} \end{bmatrix}, \tag{2.11}$$

where $\mathbf{X}^a_1$ and $\mathbf{x}^a_1$ contain the ensembles of model parameters and their mean that are estimated in the analysis step.

The ensemble of key parameters from the analysis step ($\mathbf{X}^a_1$) is used for the background step ($\mathbf{X}^b_1$) of the next time step in simulating TNDs values and the C/DA procedure continues until the observations are available.

The C/DA procedure is performed during a predefined assimilation window (see Chapter 3, section 3.2). The last set of key parameters that are estimated in this period are considered as the optimal solution, which provides us with $\hat{\Theta}_P$ in Eq. (2.12). These parameters then replace the default values of the original NRLMSISE-00 model Eq. (2.2) to now-cast and forecast (for the next hour) multi-level TNDs, individual neutral mass densities, and thermospheric temperature globally. The C/DA model, i.e., called 'C/DA-NRLMSISE-00', is represented by:

$$\text{C/DA model, i.e., } : \mathrm{F}(\hat{\Theta}_P, \Theta_R, \Theta_I), \tag{2.12}$$

which is used for providing the global multi-level TND (L3) data of this study.

2.2 Evaluation measures

To numerically evaluate the performance of the original and C/DA model (L3 data) compared to observations, the following statistical measures are applied:

- 'Bias' is defined as:

$$\text{Bias} = \frac{1}{n}\sum_{i=1}^{n}(\text{Obs}_i - \text{Model}_i), \tag{2.13}$$

  where Obs and Model denote observation and model estimates, receptively, and n is the number of observations. The positive (negative) values of the bias demonstrate that the model underestimates (overestimates) compared to observations.

- The expression of bias in percentage is computed based on the 'Relative Error (RE)' as:

$$\text{RE} = 100 \times \sum_{i=1}^{n}(\frac{|\text{Obs}_i - \text{Model}_i|}{\text{Obs}_i}), \tag{2.14}$$

  where $|.|$ represents an operator that returns absolute values.

- 'Root Mean Squared Error (RMSE)' is determined to assess how the model estimates (generally) fit to observations as:

$$\text{RMSE} = \sqrt{\frac{\sum_{i=1}^{n}(\text{Obs}_i - \text{Model}_i)^2}{n}} \tag{2.15}$$

  The square term inside the RMSE equation highlights both positive and negative differences between the quantities.

- 'Improvement' is defined as percentage in the computed RMSEs after implementing C/AD as:

$$\text{Improvement} = 100 \times \frac{\text{RMSE}_1 - \text{RMSE}_2}{\text{RMSE}_1}, \tag{2.16}$$

  where RMSE_1 is computed between the original NRLMSISE-00 and observed-TNDs, and RMSE_2 is determined between those of C/DA and observed-TNDs.

- 'Average of Absolute Percentage Deviation (AAPD)' is expressed as the percentage of absolute difference between observation and model as:

$$\text{AAPD} = 100 \times \frac{\sum_{i=1}^{n}(|\frac{\text{Obs}_i - \text{Model}_i}{\text{Obs}_i}|)}{n}, \tag{2.17}$$

  Minimum (maximum) values of AAPD correspond to the average best (worst) performance of a model in estimating TNDs.

- 'Fit' is determined as the fraction of data variance that is predicted by the model as:

$$\text{Fit} = 1 - \frac{\sqrt{\sum_{i=1}^{n}(\text{Obs}_i - \text{Model}_i)^2}}{\sqrt{\sum_{i=1}^{n}(\text{Obs}_i - \bar{\text{Obs}})^2}}, \tag{2.18}$$

  where $\bar{\text{Obs}}$ is defined as the mean value of observations. In contrast to AAPD, the minimum (maximum) values of fitting correspond to the average worst (best) performance of model in simulating TNDs.

- 'Correlation Coefficients (CCs)' are used as a unit-less measure to represent the overall agreement between the evolution of model estimations and observations:

$$\text{CC} = \frac{\sum_{i=1}^{n}(\text{Model}_i - \bar{\text{Model}})(\text{Obs}_i - \bar{\text{Obs}})}{\sqrt{\sum_{i=1}^{n}(\text{Model}_i - \bar{\text{Model}})^2 \sum(\text{Obs}_i - \bar{\text{Obs}})^2}}. \tag{2.19}$$

  The range of CCs is from -1 to $+1$, where -1 indicates the perfect negative correlation, $+1$ corresponds to the 100% correspondence, and zero indicates no correlations. It is worth mentioning that the computational values of CCs may be bigger than $+1$ or smaller than $-l$, which only reflect the uncertainties of the estimation and they cannot be interpreted,

- 'Coefficient Of Efficiency (COF)' is used as a unit-less measure to assess the performance of model simulations compared to observations as:

$$\text{COF} = 1 - \frac{\sum_{i=1}^{n}(\text{Obs}_i - \text{Model}_i)^2}{\sum_{i=1}^{n}(\text{Obs}_i - \bar{\text{Obs}})^2}. \tag{2.20}$$

  The minimum (maximum) values of COF correspond to the average worst (best) performance of the models.

CHAPTER 3

Results

3.1 Selecting the storm periods

The space missions CHAMP, GRACE, GOCE, Swarm, and GRACE-FO cover the years of 2000-2010, 2002-2017, 2009-2013, 2013-now, and 2018-now, respectively. Measurements of these missions are used within the C/DA experiments to study their feasibility for generating global multi-level L3 TND data sets. For our investigations, periods with considerable geomagnetic activity, i.e., with considerable K_p fluctuations, are extracted. Seven periods are chosen based on the coverage of these missions, where they are among strong geomagnetic storm periods during 2003-2020. The corresponding geomagnetic changes are shown in figure 3.1. The corresponding dates where the pronounced geomagnetic activity is observed are listed in Table 3.1, i.e., Storm1 (2003-10-28:31), Storm2 (2004-07-21:29), Storm3 (2008-03-25:29), Storm4 (2010-04-03:07), Storm5 (2015-03-15:26), Storm6 (2017-09-06-09), and Storm7 (2020-09-23:29). The average of K_p in these storms is 6, 4, 3, 4, 3, 3, and 3. The range of differences in them is found to be considerably different, i.e., 4-8, 1-8, 1-5, 1-8, 2-8, 1-8, and 2-6.

Table 3.1: An overview of the space-based TND measurements used as observation within the C/DA to produce the global multi-level L3 products, and those that are used for validation.

Number	Date	Assimilation mission Average Height (km)	Validation mission Average Height (km)
Storm1	2003-10-28:31	CHAMP (401.13)	GRACE (490.91)
Storm2	2004-07-21:29	CHAMP (386.60)	GRACE (486.34)
Storm3	2008-03-25:29	GRACE (477.74)	CHAMP (343.75)
Storm4	2010-04-03:07	CHAMP (301.59)	GOCE (270.03)
Storm5	2015-03-15:26	Swarm-C (466.86)	Swarm-B (520.69)
Storm6	2017-09-06-09	Swarm-C (451.35)	Swarm-B (514.80)
Storm7	2020-09-23:29	Swarm-C (444.48)	Swarm-B (512.72)

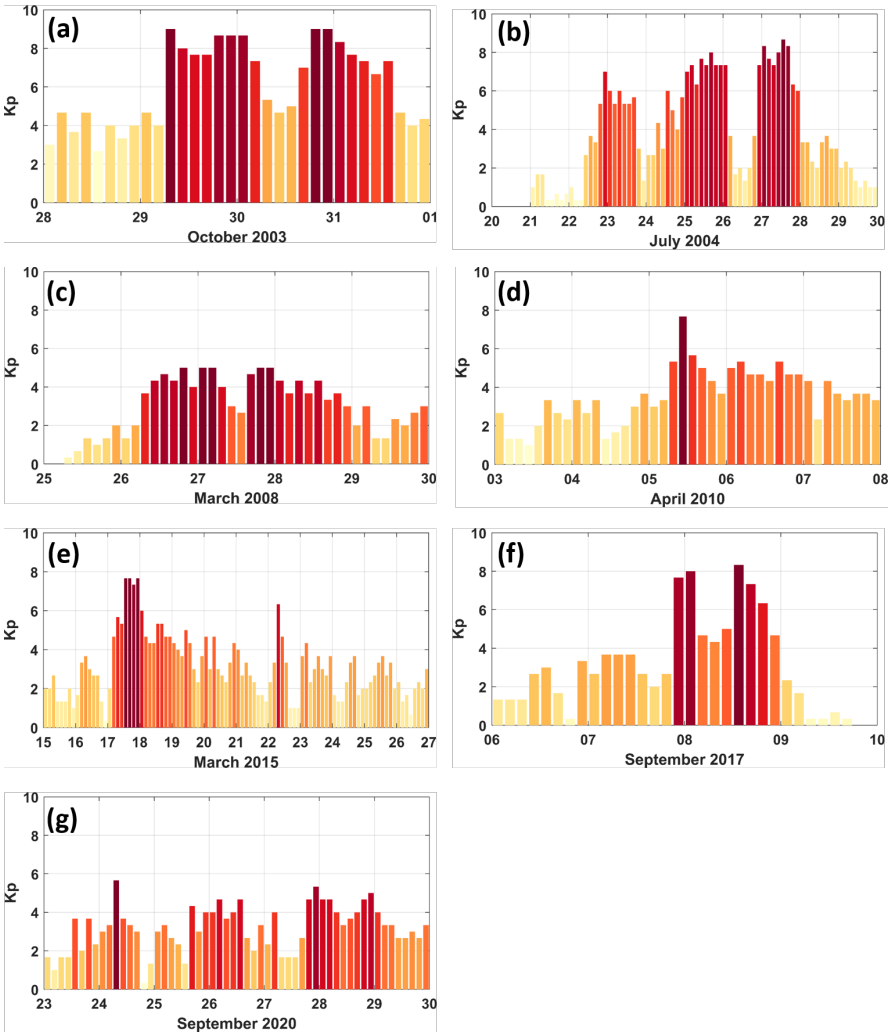

Figure 3.1: An overview of the geomagnetic activity, represented by the (Kp) index during the seven periods (between 2003-2020) selected by this study.

3.2 Selecting the assimilation window

To determine a suitable assimilation window size, which minimises the errors of TND predictions during one hour after the C/DA (i.e., during the forecast phase), 22 experiments are implemented. In each experiment, we changed the assimilation window from 1 hour to 22 hours, and the calibrated parameters were used to predict the TNDs

of 23:00:00 UT to 23:59:30 UT on October 29^{th}, 2003. The maximum improvement in the RMSE values (Eq. 2.15) of the TND forecasts demonstrates the optimal assimilation window. As observation, the TND estimates of CHAMP are applied. Figure 3.2 indicates the improvements for the assimilation windows (of 1 to 22 h). These results indicate that the optimal choice to perform a successful fitting is around 3 hours, and this is used for the entire C/DA experiments of this project. We also noticed that the assimilation window of 1 to 4 hours would provide acceptable results (i.e., no big changes were detected in the RMSE). However, selecting longer assimilation window would negatively affect the forecasting results. This is likely because the temporal correlations between the temporal TND changes and the estimated values of model parameters is only high over short periods, and old observations would only add more uncertainty to the system rather than improving the parameter estimation within the EnKF procedure.

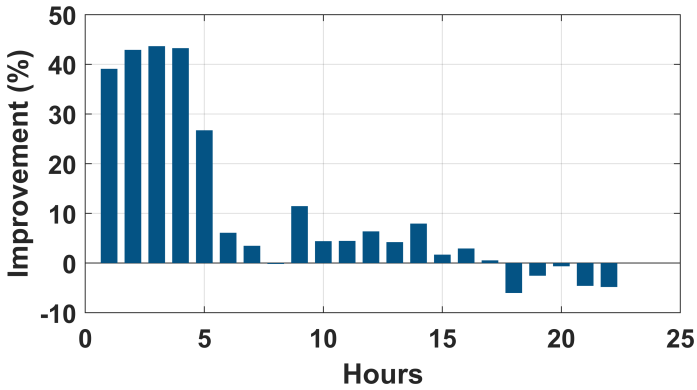

Figure 3.2: An overview of the improvements in forecasting TNDs during October 29^{th}, 2003. The results are estimated by running the original NRLMSISE-00 and C/DA-NRLMSISE-00. The C/DA is processed using the TND estimates of CHAMP as observation, then the calibrated parameters derived from different assimilation windows are used to form the C/DA-NRLMSISE-00 model and forecast the TNDs along the orbit of CHAMP.

3.3 The choice of sampling

To properly select sampling for producing the L3 TND data, we took advantage of empirical covariance matrices. This investigation is separated for the temporal and spatial sampling, which is described in what follows.

3.3.1 Temporal sampling

To find optimum temporal sampling, the n grid points (in each TND map) at m time epochs are arranged into an m by n data matrix. The temporal mean of this data matrix is $\bar{\mathbf{y}}_{p,1} = \frac{1}{n}\sum_{i=1}^{n} \mathbf{r}_{p,i}$ where $p = 1, \ldots, n$, and each element of $\bar{\mathbf{y}}$ is the mean value of all n observations for m grid points. The deviations of all observations from their mean value are arranged into an $m \times n$ matrix, $\mathbf{Y} = [\mathbf{y}'_1, \mathbf{y}'_2, \ldots, \mathbf{y}'_n]$. The empirical covariance matrix $\mathbf{C}$ can be written as:

$$\mathbf{C} = \frac{1}{m}\mathbf{Y}\mathbf{Y}^T, \tag{3.1}$$

where the superscript T represents the transpose operator. The covariance matrix is converted to the equivalent correlation values by dividing the entries by the estimated variance values. The global temporal correlation is shown in figure 3.3. The results indicate that the temporal sampling that corresponds to the high correlation value of 0.95 is about 1 hour. Since this value may be different for each grid point, we also repeated this assessment for 63536 grid points globally and computed the auto-correlation value. By considering 0.95 as a high correlation threshold, we extracted the smallest temporal lags, which are presented in figure 3.4 showing that the temporal lag of 45 minutes is an optimum temporal sampling for 40% of the TND grid points. We also display the auto-correlation map of lags 45 and 60 minutes in figure 3.5, which shows by producing 1 hourly TND products we do not loose too much information. The time interval of 1 hour seems to be suitable for producing the global L3 TND products.

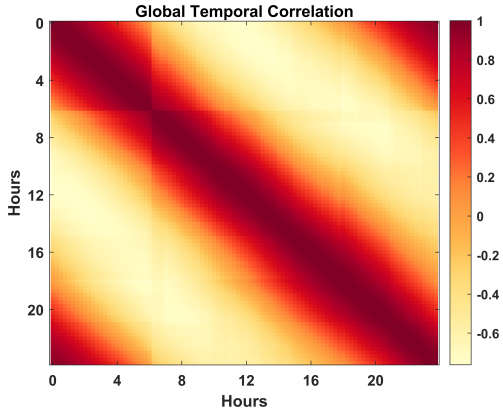

Figure 3.3: An overview of temporal correlations that are computed using 24 hours of TND data during October 29^{th}, 2003. The global 1 degree TND maps are estimated at 400 km with the temporal sampling of 15 minutes. The results indicate that the temporal correlations with the time lag of less than four hours are high.

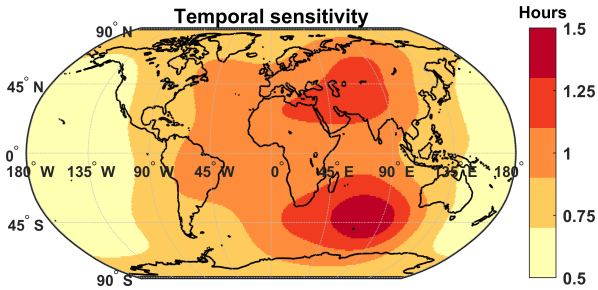

Figure 3.4: Temporal lags that correspond to the correlation coefficient of 0.95. Results are generated using the auto-correlation function applied on 1 degree TND grid points during 24 hours of October 29^{th}, 2003.

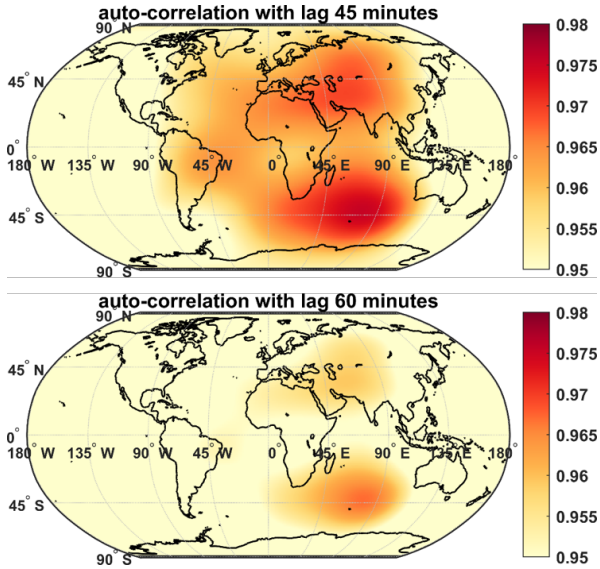

Figure 3.5: The auto-correlation values with the temporal lags 45 and 60 minutes.

3.3.2 Spatial sampling

To find an optimum spatial sampling to produce global TND products, we analysed the spatial empirical covariance matrices that were built for latitudinal and longitudinal TND changes, individually. To illustrate the sensitivity with respect to latitude, we show the estimation for the longitude of 150°, where the latitudes vary between -90 and 90°, see figure 3.6,(a). Figure 3.6,(b) shows the empirical covariance matrix when the values lower than 0.98 are masked. Analogous to latitude sensitivity, we investigate the longitude sensitivity. As an example, figure 3.6,(c) presents the results for the latitude of 60.5° and the longitudes vary from -180 to 180°. The masked covariance matrix with 0.98 being chosen as high CC threshold is depicted in figure 3.6,(d). Considering these estimates globally, we concluded that the spatial sensitivity is around five degrees.

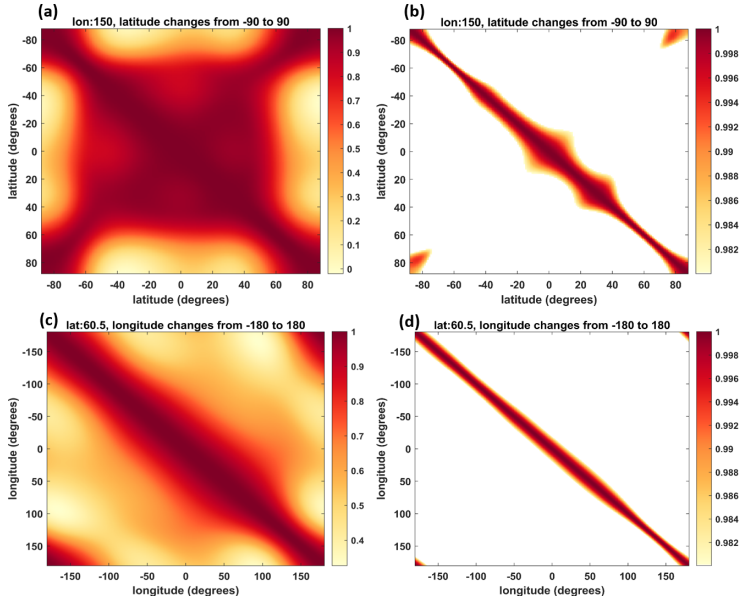

Figure 3.6: An overview of the spatial sensitivity derived by computing the empirical covariance matrices along latitudes and longitudes. The example corresponds to the longitude of 150° (a and b), and the latitude of 60.5° (c and d).

3.3.3 Altitude sensitivity

To determine an optimum altitude resolution for the global maps, we fitted exponential functions to the simulated TNDs derived from C/DA-NRLMSISE-00 at 12 UT on October 29^{th}, 2003 covering 150 km to 550 km at 1 km vertical intervals. Then, we repeated this curve fitting experiments with increasing the distance of intervals from 1 to 100 km. We selected 0.9 as a fitting threshold to define considerable changes derived be the miss-sampling of the vertical information. Figure 3.7 presents these values indicating that, on the average, a vertical sampling of 25 km can be considered to present the multi-level products without loosing too much vertical information.

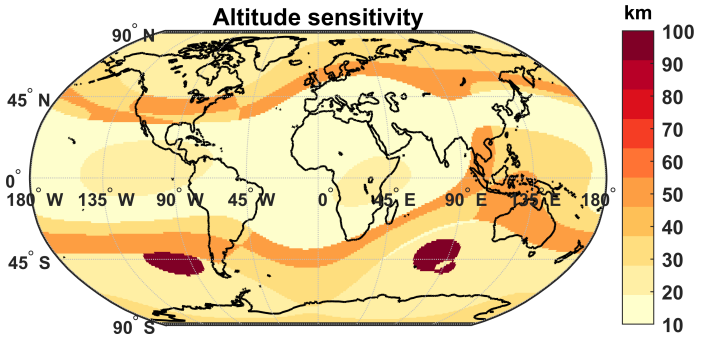

Figure 3.7: The magnitude of altitudes, where considerable changes in the shape of vertical profile is detected. The experiment is done at 12 UT on October 29^{th}, 2003.

3.4 Investigations during events with considerable geomagnetic activity

In what follows, the outputs derived from C/DA-NRLMSISE-00 are investigated during seven events with considerable geomagnetic activity. We call these events 'Storm' and therefore they are named as 'Storm1 to 7' in this report. The satellite mission data used for performing the C/DA and validation are summarised in Table 3.1. We also compared the TND estimates of C/DA with those of the original NRLMSISE-00 model, as well as the JB08, and the HASDM models. The presented results of this chapter are in the forecasting mode, it means that the C/DA-NRLMSISE-00 has already been preformed using the TND data of three hours before and the satellite derived TNDs that we show in each figure are not used within the C/DA. Therefore, one may argue that the C/DA results are validated against satellite measurements. The forecasting mode is also selected here to demonstrate the value of L3 data for prediction studies, once the production chain of the space-based along track TNDs and L3 production is changed to be (near) real-time.

3.4.1 Evaluation during Storm1, October 2003

In this experiment, we performed the C/DA using CHAMP data of October 28^{th}-31^{st}, 2003 as observation. Figure 3.1,(a) shows the geomagnetic index, which is represented by the K_p from `ftp://ftp.ngdc.noaa.gov/STP/GEOMAGNETIC_DATA/INDICES/KP_AP`. The average K_p during the selected four days are 3.7, 7.2, 7, and 6.2, respectively. Considering the Kp anomalies, one can consider October 29^{th} and 30^{th} to be the main storm days.

Validations of this experiment are carried out along both CHAMP and GRACE orbits that are shown in figure 3.8 (top and bottom) and the statistical comparisons are provided in Table 3.2 and Table 3.3, respectively. The numerical results indicate that, compared to other models, the C/DA estimates are closer to the CHAMP and GRACE measurements. The improvement is seen for both correlation coefficients and the relative error measures, which shows that the overall consistency and local fluctuations of the C/DA estimates are close to the satellite derived TND estimates.

Table 3.2: A summary of statistical measures between the NRLMSISE-00, JB08, HASDM, and the TND forecasts of C/DA-NRLMSISE-00 compared to the TND estimates of CHAMP during Storm1 in October 2003.

Model	RMSE (kg/m^3)	Bias (kg/m^3)	Coefficient Of Efficiency	Correlation	AAPD (%)	RE(%)
NRLMSISE-00	5.08×10^{-12}	4.28×10^{-12}	-3.50	0.43	74.87	84.31
JB08	2.52×10^{-12}	1.49×10^{-12}	-0.10	0.57	31.22	41.79
HASDM	2.37×10^{-12}	1.49×10^{-12}	0.01	0.60	27.22	38.51
C/DA-NRLMSISE-00	1.74×10^{-12}	5.79×10^{-14}	0.46	0.72	21.64	28.99

Figure 3.9 presents scatter plots of the orbit averaged TNDs from the original NRLMSISE-00, JB08, HASDM, and C/DA-NRLMSISE-00 against the assimilated

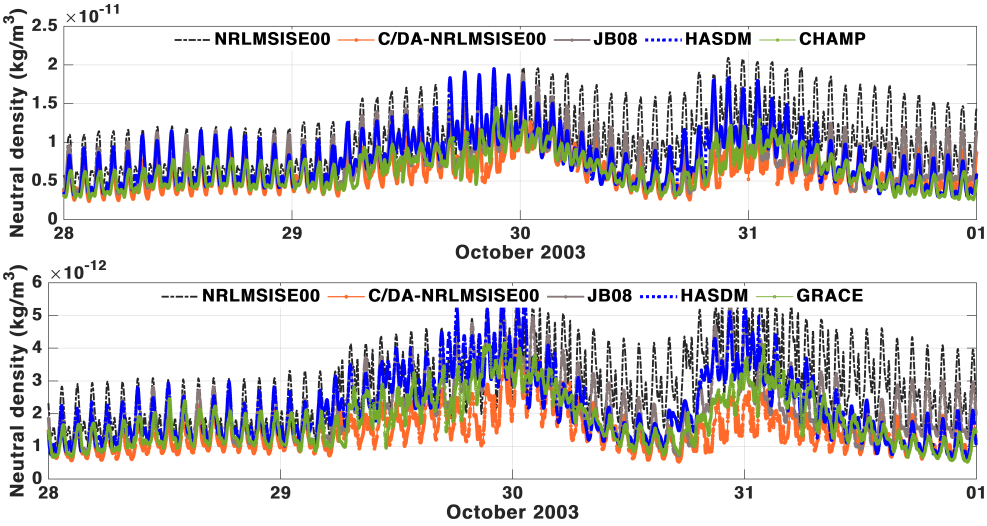

Figure 3.8: A comparison between the TND forecasts of C/DA-NRLMSISE-00 and those of the original NRLMSISE-00 model, as well as JB08, HASDM models along the CHAMP (top) and GRACE (bottom) orbits. The C/DA is processed using CHAMP measurements as observation using 3 hours assimilation window. The C/DA results are in the forecast mode.

Table 3.3: A summary of statistical measures between the NRLMSISE-00, JB08, HASDM, and the TND forecasts of C/DA-NRLMSISE-00 compared to the TND estimates derived from GRACE measurements during Storm1.

Model	RMSE (kg/m^3)	Bias (kg/m^3)	Coefficient of Efficiency	Correlation	AAPD (%)	RE(%)
NRLMSISE-00	1.28×10^{-12}	1.03×10^{-12}	-1.43	0.54	71.15	57.91
JB08	6.74×10^{-13}	3.47×10^{-13}	0.32	0.68	32.35	30.49
HASDM	6.75×10^{-13}	3.56×10^{-13}	0.32	0.66	28.06	29.76
C/DA-NRLMSISE-00	6.16×10^{-13}	-3.34×10^{-13}	0.43	1.03	22.46	27.84

and validation data in the analysis (during the fitting period of C/DA) and the forecast (during prediction using the adjusted model parameters) modes. The results indicate that in all cases the C/DA results have a better consistency (see the 'R' values) with space-based measurements than other available models. The pots also show that the results in both modes are indeed better than the existing models. The quality of the forecast is not found to be considerably worse than the analysis mode, which can be considered as a positive indication for using the presented C/DA technique for prediction applications.

To investigate the dominant spatial and temporal differences between multi-level TND estimates of the C/DA-NRLMSISE-00 and the original NRLMSISE-00 model,

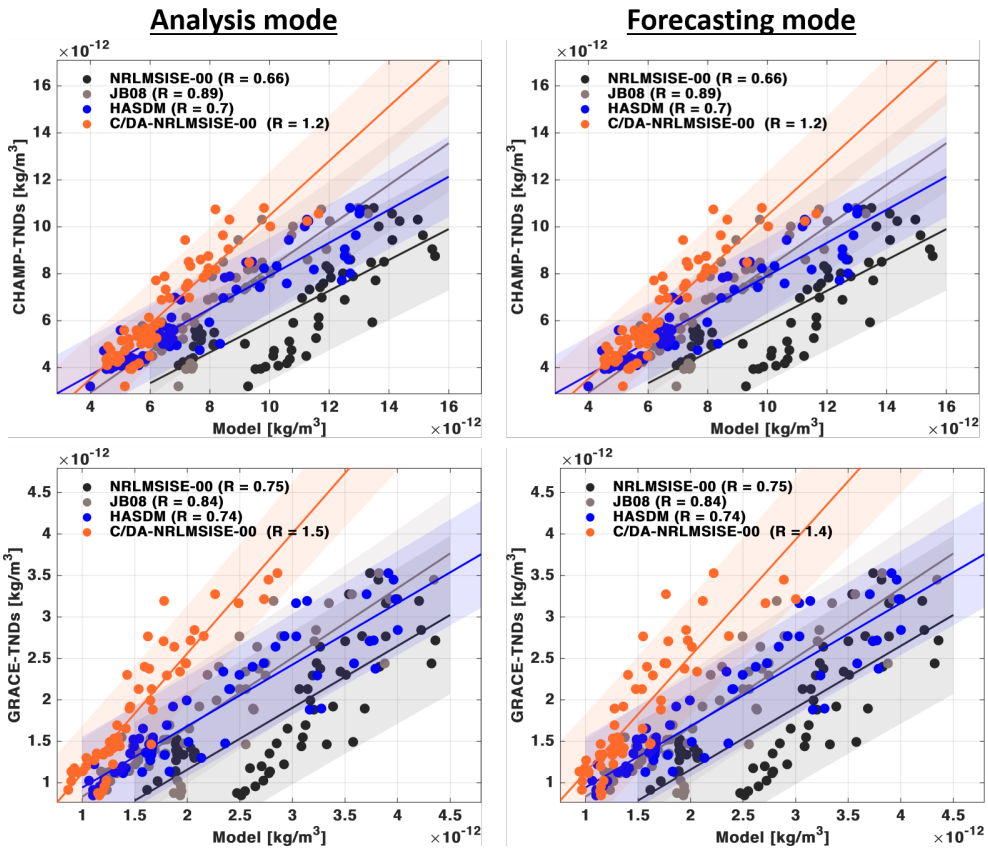

Figure 3.9: Scatter-plots of the TND during Strom1 in October 2003. The full day orbit averaged CHAMP and GRACE TNDs are considered against the TND estimated of the original NRLMSISE-00, JB08, HASDM model estimates, as well as those of the C/DA-NRLMSISE-00.

the Principal Component Analysis (PCA, [27]) method is applied. At the first step, for the entire period of Storm1, PCA is applied on the half hourly, global, 1 degree resolution TND maps of NRLMSISE-00 and C/DA NRLMSISE-00 at altitude of 450 km. This altitude chosen as an arbitrary example, where the value is between those of the CHAMP and GRACE orbital altitudes during the period of Storm1.

As a result of PCA, the spatial patterns are extracted that are known as the Empirical Orthogonal Functions (EOFs, i.e., anomaly maps in terms of density kg/m^3) and their associated uncorrelated temporal patterns (Principal Components, or PCs, which are unit-less). These statistical components represent the orthogonal modes

that are, for example, plotted in figure 3.10. Then, PCA is applied on the differences between the original NRLMSISE-00 and C/DA-NRLMSISE-00 in the forecasting mode. The average and standard deviation of spatial differences, along with the first two dominant modes of the PCA of differences are shown in figure 3.11.

The PCA results of figure 3.10 indicate that on 450 km altitude the dominant TND differences are related to those changes caused by the geomagnetic activity (64% of the total variance), where the original model falls short in reflecting these changes, i.e., the anomalies of EOF1 and the magnitude of PC1 are found to be different. Those of C/DA follow geomagnetic activity index and the corresponding TND changes are closer to observations, see, e.g., figure 3.9. We found less dominant changes on daily time scale that correspond to 17% of the total variance. The differences shown in figure 3.11 indicate that a bias at the order of $\sim 1.8 \times 10^{-12}$ kg/m^3 can be expected from the original NRLMSISE-00 model during Storm1 (see the top-left plot) and a standard deviation of $\sim 1 \times 10^{-12}$ kg/m^3 for estimating the temporal fluctuations (see the top-right plot). By confirming the results of figure 3.11, the PCA of differences (plots on the middle and bottom of figure 3.11) indicates that the dominant differences, after applying the C/DA, correspond to the TND changes caused by the geomagnetic activity, i.e., (82% of the variance of the differences). The magnitude of differences on the daily time scale is found to be at the range of $\sim 6 \times 10^{-13}$ kg/m^3 at 450 km altitude, i.e., equivalent with 17% of the total variance of differences in TNDs.

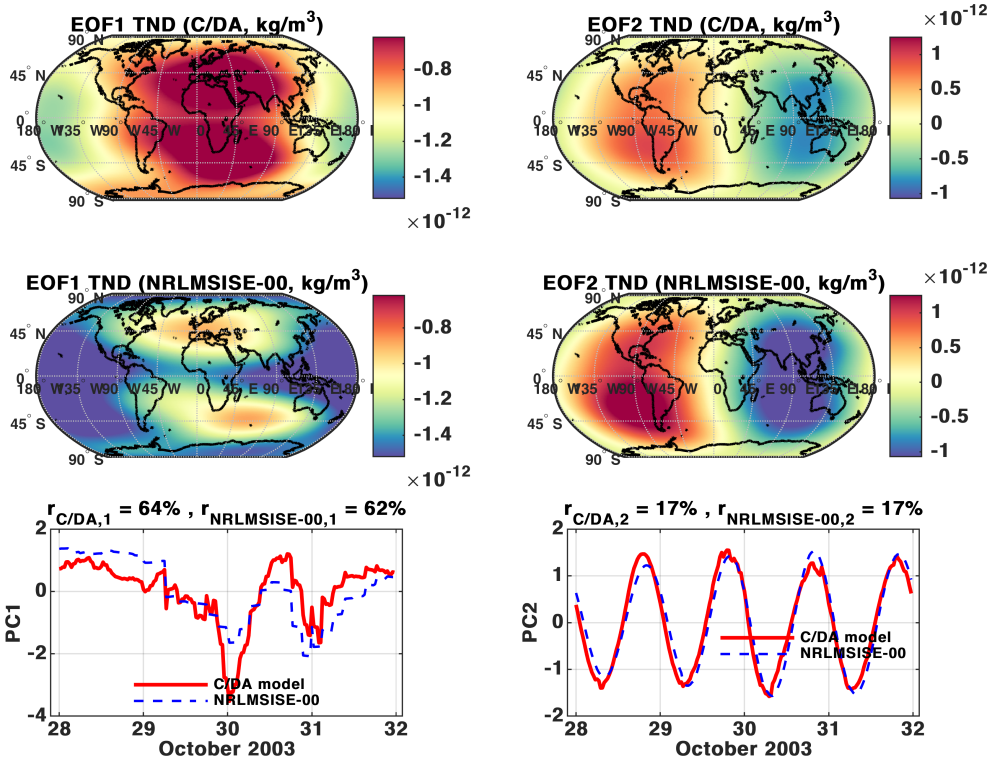

Figure 3.10: An overview of the PCA results applied on the TND estimates of NRLMSISE-00 and C/DA-NRLMSISE-00 at 450 km during Storm1 in October 2003. The anomaly maps (EOFs) are in terms of kg/m^3, which can be multiplied by the unit less time series (PCs) on the bottom to derive the PCA orthogonal modes. The first orthogonal mode represents around 62% of the total variance of TND changes and the second mode indicates around 17%.

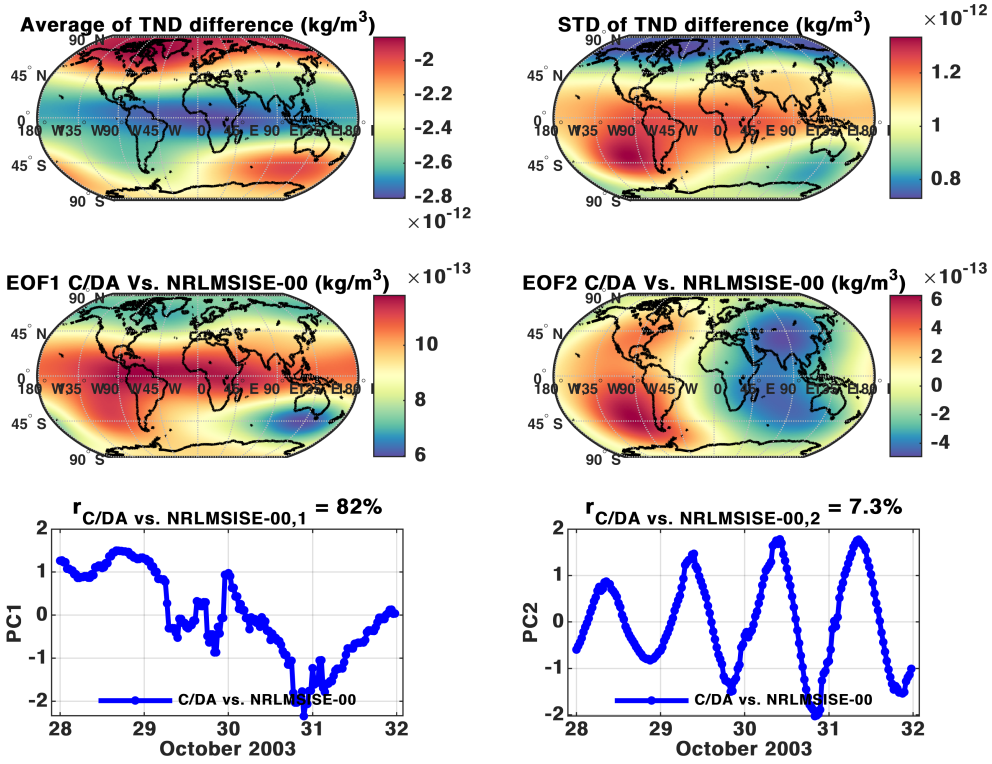

Figure 3.11: PCA of the TND differences between NRLMSISE-00 and C/DA-NRLMSISE-00 at 450 km during Storm1 in October 2003. The anomaly maps (EOFs) are in terms of kg/m^3, which can be multiplied by the unit less time series (PCs) on the bottom to derive orthogonal modes. The first mode of differences represents 82% of the total variance of TND differences and the second mode indicates 7.3% of the variance.

3.4.2 Evaluation during Storm2, July 2004

During the period of Storm2 in 2004, CHAMP data was applied as observation. Figure (3.1,b) shows the corresponding geomagnetic changes. The results are investigated in the forecasting mode and the TND data of CHAMP and GRACE are applied for validation.

Figure 3.12 shows the results, where the correlation coefficients of 72(80), 79(89), 68(70), and 91(102)% are found between the original NRLMSISE-00 / JB08 / HASDM / the forecast mode of C/DA-NRLMSISE-00 and those TND estimates along track of the CHAMP (GRACE). More statistical details are provided in Table 3.4 and Table 3.5.

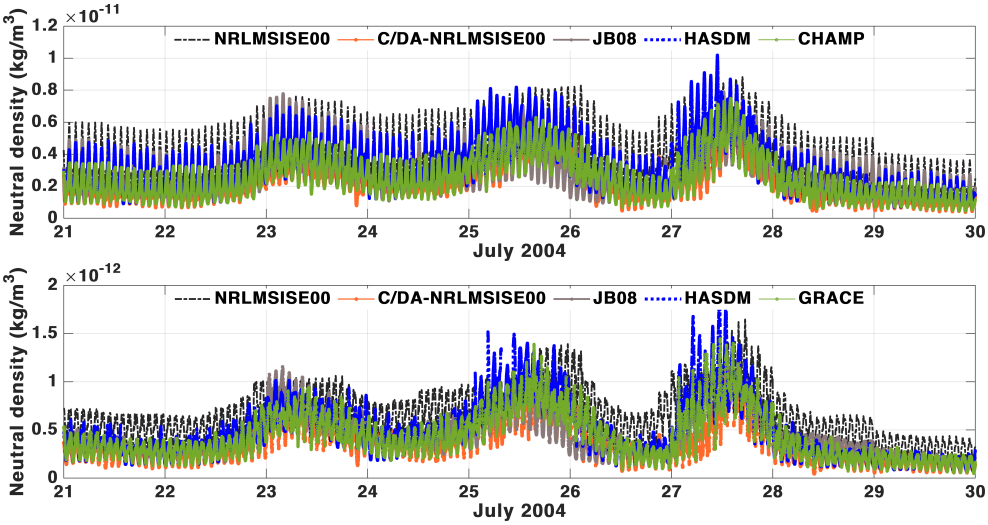

Figure 3.12: A comparison between the TND forecast of C/DA-NRLMSISE-00 and those derived from the NRLMSISE-00, JB08, and HASDM models along the CHAMP (top) and GRACE (bottom) tracks during July 2004. The C/DA is processed using CHAMP data as observation, then the C/DA-NRLMSISE-00 TNDs are evaluated along the CHAMP and GRACE orbits.

To investigate the dominant spatial and temporal changes caused by applying the C/DA method during July 21^{st}-29^{th}, 2004, PCA is applied on the half hourly global TNDs derived from NRLMSISE-00 and C/DA-NRLMSISE-00 at the altitude of 350 km. This altitude is chosen to be different from the altitude of Storm1, and at the same time, to be close to the altitude of CHAMP during this period. However, this choice does not affect the overall conclusion of this experiment and by selecting any altitudes between 300-500 km (that we tested) similar spatial and temporal compo-

Table 3.4: A summary of statistical measures between the TNDs of NRLMSISE-00, JB08, HASDM, and C/DA-NRLMSISE-00 compared to the TNDs derived from CHAMP during July 21-29, 2004.

Model	RMSE (kg/m^3)	Bias (kg/m^3)	Coefficient Of Efficiency	Correlation	AAPD (%)	RE(%)
NRLMSISE-00	1.63×10^{-12}	1.41×10^{-12}	-0.45	0.72	68.50	100.34
JB08	0.83×10^{-12}	3.41×10^{-13}	0.61	0.79	28.08	51.63
HASDM	1.01×10^{-12}	6.30×10^{-13}	0.42	0.68	30.59	61.16
C/DA-NRLMSISE-00	0.61×10^{-12}	-9.39×10^{-14}	0.79	0.91	17.83	37.75

Table 3.5: A summary of statistical measures from the TNDs of NRLMSISE-00, JB08, HASDM, and C/DA-NRLMSISE-00 compared to the TNDs derived from GRACE during July 21-29, 2004.

Model	RMSE (kg/m^3)	Bias (kg/m^3)	coefficient of efficiency	Correlation	AAPD (%)	RE(%)
NRLMSISE-00	2.89×10^{-13}	2.55×10^{-13}	-0.33	0.80	79.94	82.20
JB08	1.37×10^{-13}	1.31×10^{-14}	0.69	0.89	24.47	39.12
HASDM	1.59×10^{-13}	6.77×10^{-14}	0.58	0.70	25.28	44.64
C/DA-NRLMSISE-00	1.42×10^{-13}	-6.65×10^{-14}	0.67	1.03	20.28	50.51

nents were extracted. The magnitude of their modes however was different because TND decreases by increasing the altitude.

The first two dominant of EOFs and PCs are presented in figure 3.13. PCA is also performed on the differences between the original NRLMSISE-00 and the C/D-NRLMSISE-00 in the forecasting mode. The average and standard deviation of the spatial differences along with the first two dominant modes of the PCA of differences are shown in figure 3.14. The minimum and maximum magnitude of the first mode reach up to $-3.07\times10^{-12}kg^{m3}$ (65% of the total variance), and $1.68\times10^{-12}kg^{m3}$ (15% of the total variance), respectively. Here, the magnitude is computed by multiplying the maximum value of the EOFs with the maximum value of their corresponding PCs.

Similar EOF1 and PC1 are found from the original NRLMSISE-00 and C/DA-NRLMSISE-00 (figure 3.13), but PC1 of C/DA shows different (a delayed) response to the storm condition, i.e., on July 27^{th}, PC1 of the two models are different. The main differences in the second mode (EOF2 and PC2) are found to be related to daily TND changes. The differences shown in figure 3.14 indicate that a bias on the order of $\sim 2.5\times10^{-12}$ kg/m^3 can be expected by applying the NRLMSISE-00 model during Storm2 (see the top-left plot) and a standard deviation of $\sim 1\times10^{-12}$ kg/m^3 for estimating the temporal fluctuations (see the top-right plot).

The PCA of differences confirms the results of figure 3.14. Plots on the middle and bottom of figure 3.14 show the first two dominant PCA modes, where the first is related to the TND response to Storm2 (e.g., see PC1 around July 27^{th}, where the first mode corresponds to 78% of the total variance of differences). The second mode (EOF2 and PC2) shows both daily and half-daily TND differences on the order of $\sim 10^{-13}$ kg/m^3 at 350 km altitude, i.e., equivalent with 5.7% of the total variance of TND differences.

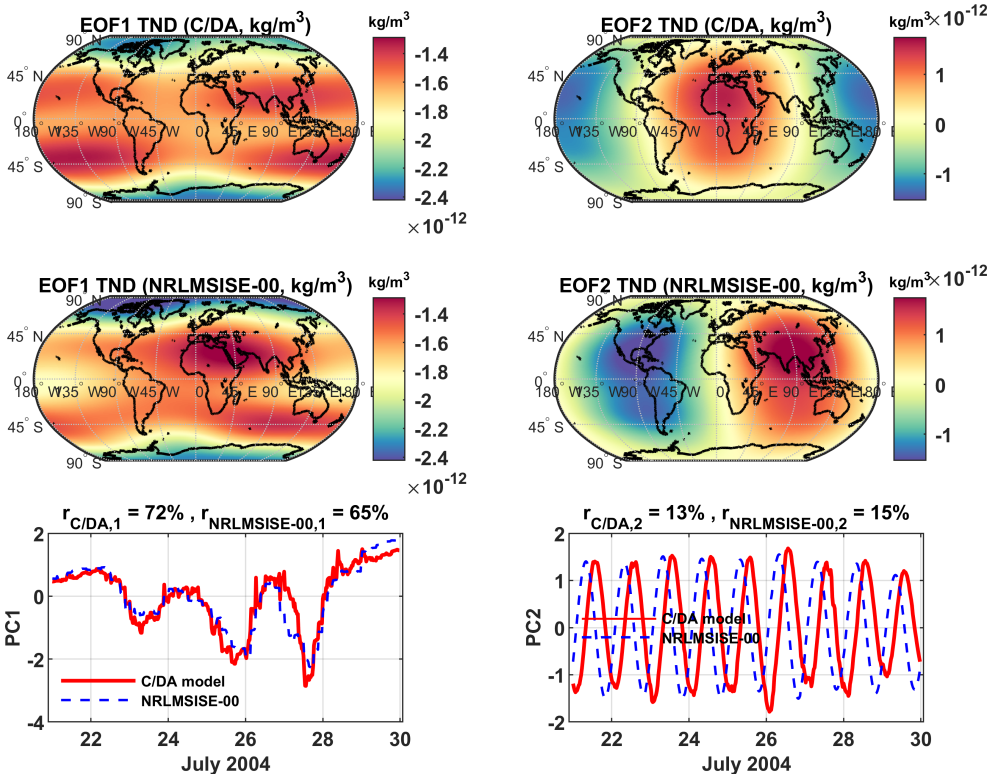

Figure 3.13: An overview of the PCA results applied on the global TND estimates of the original NRLMSISE-00 and the forecast values of C/DA-NRLMSISE-00 at 350 km during July 2004. The anomaly maps (EOFs) are in terms of kg/m^3, which can be multiplied by the unit less time series (PCs) to derive the orthogonal modes. The variances are reported on the top of the PC plots.

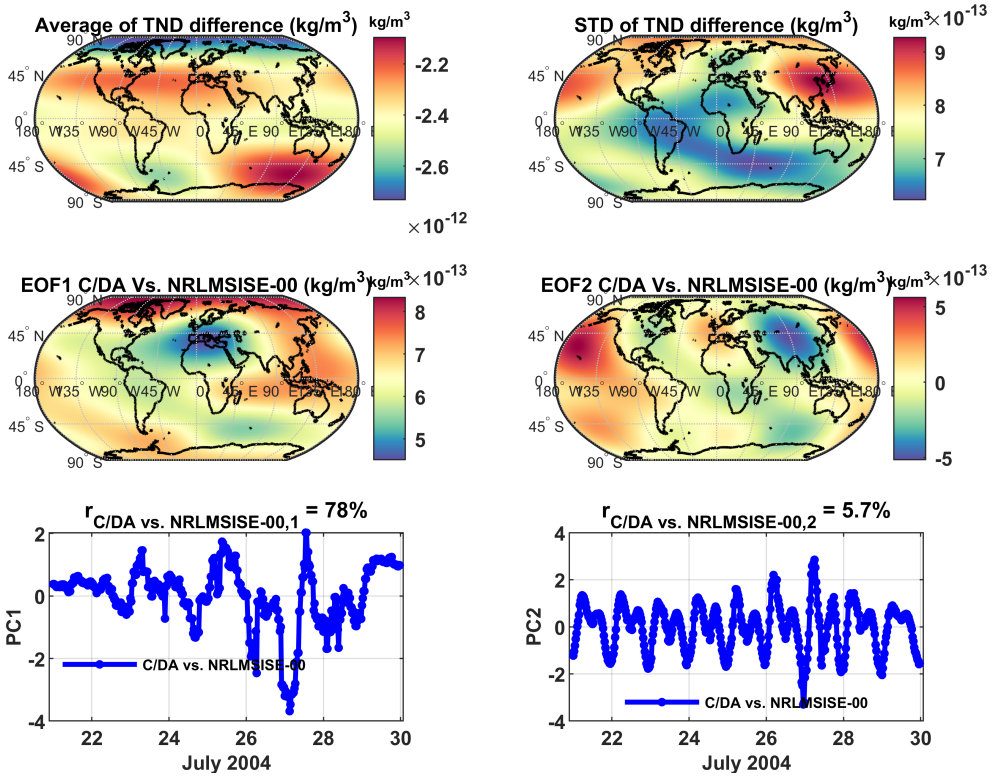

Figure 3.14: An overview of the PCA implementation on the TND differences derived between the original NRLMSISE-00 and C/DA-NRLMSISE-00 in the forecasting mode and at the altitude of 350 km during July 2004. The anomaly maps (EOFs) are in terms of kg/m^3, which can be multiplied by the unit less time series (PCs) on the right to derive orthogonal modes. The total variance of the TND differences are reported on the top of the PC plots.

3.4.3 Evaluation of Storm3, March 2008

During Storm3, March 25^{th}-29^{th}, 2008, GRACE measurements are used for performing the C/DA, where both CHAMP and GRACE are used to evaluate the predictions. The corresponding geomagnetic activity during this period can be found in figure (3.1,c).

The along track results are shown in figure 3.15, where various statistical measured are reported in Table 3.6 and Table 3.7 presenting the results along the GRACE and CHAMP orbits, respectively. In both validation attempts, the C/DA results indicated better results, for example, the correlation coefficients between the original NRLMSISE-00 / JB08 / HASDM / the C/DA-NRLMSISE-00 in the forecasting mode and the measured TNDs along the GRACE (CHAMP) orbits are found to be 67(73), 69(72), 73(63), and 84(84)%. This indicates the overall high correspondence of the C/DA estimates to the space-based measurements. We skip showing the PCA results of the global TND maps during this storm because no new conclusions rather than observing a global disagreement in representing changes due to geomagnetic activity and diurnal/semi-diurnal time scales could be drawn.

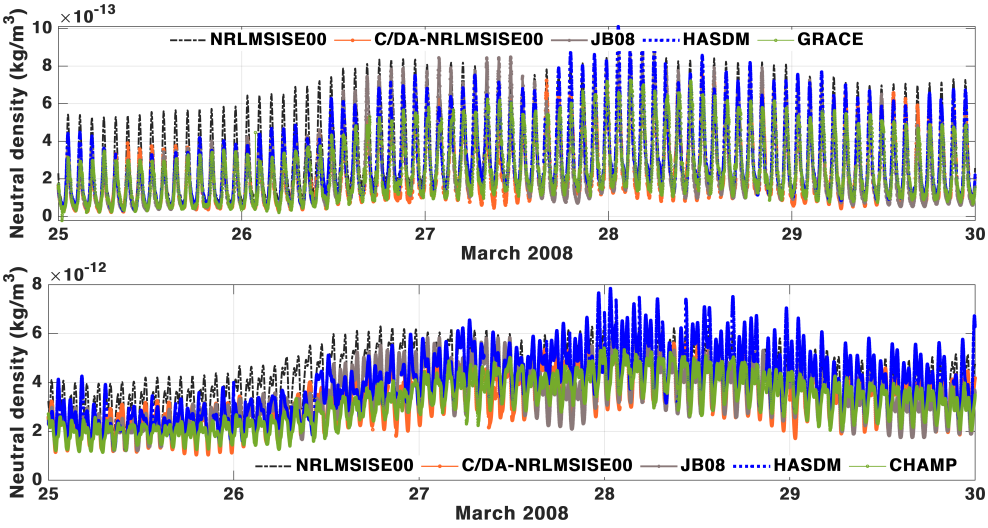

Figure 3.15: A comparison of the time series of TND estimates derived from the original NRLMSISE-00, JB08, HASDM, and C/DA-NRLMSISE-00 models along with GRACE (top) and CHAMP (bottom) TNDs. The C/DA is processed using GRACE measurements as observation, then the C/DA-NRLMSISE-00 densities are evaluated in the forecasting mode along the orbits of CHAMP and GRACE.

Table 3.6: A summary of the statistical measures derived between the original NRLMSISE-00 model, JB08, HASDM, and the C/DA-NRLMSISE-00 in the forecast mode compared to the TND measurements derived from GRACE during March 2008.

Model	RMSE (kg/m^3)	Bias (kg/m^3)	Coefficient Of Efficiency	Correlation	AAPD (%)	RE(%)
NRLMSISE-00	1.33×10^{-13}	8.90×10^{-14}	0.31	0.67	46.44	47.33
JB08	9.94×10^{-14}	1.21×10^{-14}	0.62	0.69	27.88	35.30
HASDM	9.62×10^{-14}	4.22×10^{-14}	0.64	0.73	27.75	33.59
C/DA-NRLMSISE-00	6.72×10^{-14}	-1.93×10^{-15}	0.82	0.84	21.89	23.87

Table 3.7: A summary of the statistical measures derived between the original NRLMSISE-00 model, JB08, HASDM, and the C/DA-NRLMSISE-00 in the forecast mode compared to the TND measurements derived from CHAMP during March 2008.

Model	RMSE (kg/m^3)	Bias (kg/m^3)	coefficient of efficiency	Correlation	AAPD (%)	RE(%)
NRLMSISE-00	1.21×10^{-12}	1.01×10^{-12}	-0.46	0.73	37.93	45.66
JB08	6.97×10^{-13}	2.40×10^{-13}	0.51	0.72	17.82	26.25
HASDM	1.09×10^{-12}	8.20×10^{-13}	-0.19	0.63	28.38	40.24
C/DA-NRLMSISE-00	5.33×10^{-13}	1.89×10^{-13}	0.71	0.84	14.84	20.08

3.4.4 Evaluation during Storm4, April 2010

During the period of Storm4 (April 3^{rd}-7^{th}), 2010), the TND measurement of CHAMP were used as observation to produce the C/DA model. Figure (3.1,d) displays the corresponding changes in geomagnetic activity shown by the K_p index.

For validation, hourly forecasts of TNDs along CHAMP and GOCE are considered. Figure 3.16 represents the times-series of TNDs. From the numerical measures, the correlation coefficients between the original NRLMSISE-00 / JB08 / HASDM / C/DA-NRLMSISE-00 and the measured TNDs along CHAMP (GOCE) are found to be 16(63), 17(64), 22(58), and 25(71)%, which indicate an overall improvement in the estimation of the evolution of TNDs along these two satellite missions. In addition, Table 3.8 and Table 3.9 summarise various statistical measures during Storm4 along the CHAMP and GOCE, respectively, where those of C/DA are in the forecast mode.

Table 3.8: A summary of the statistical measures derived for the original NRLMSISE-00, JB08, HASDM, and C/DA-NRLMSISE-00 compared to the TNDs derived from the CHAMP measurements during April 2010.

Model	RMSE (kg/m^3)	Bias (kg/m^3)	Coefficient Of Efficiency	Correlation	AAPD (%)	RE(%)
NRLMSISE-00	5.37×10^{-12}	2.98×10^{-12}	-3.18	0.16	43.92	58.44
JB08	5.31×10^{-12}	2.42×10^{-12}	-3.09	0.17	40.83	57.82
HASDM	6.01×10^{-12}	3.99×10^{-12}	-4.26	0.22	47.70	64.40
C/DA-NRLMSISE-00	4.02×10^{-12}	7.33×10^{-13}	-1.34	0.25	31.19	43.77

To provide an overview of the global TND changes in (relatively) low altitudes, PCA is applied on the half hourly global TND maps derived from the original NRLMSISE-00 and C/DA-NRLMSISE-00 at the altitude of 150 km. The correspond-

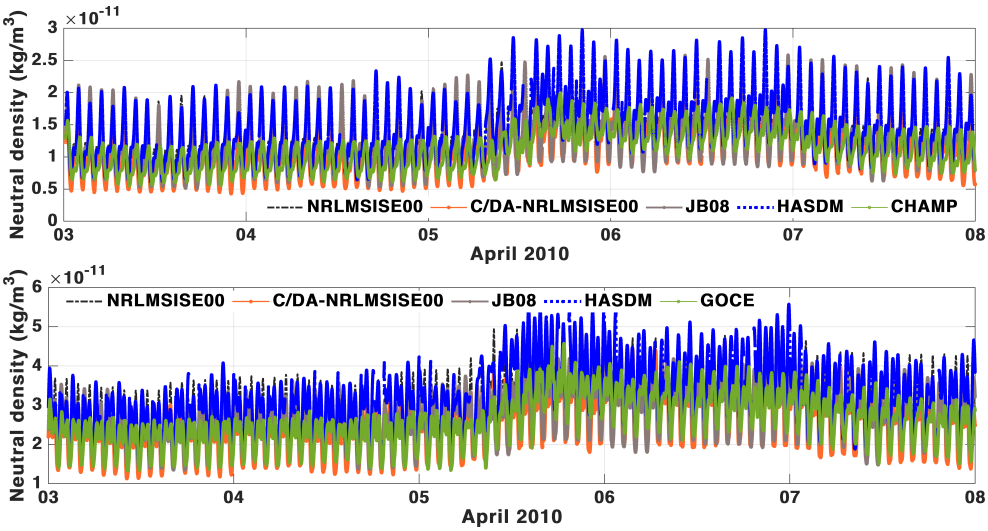

Figure 3.16: An overview of the TND estimates derived from the NRLMSISE-00, JB08, HASDM, and C/DA-NRLMSISE-00 models along the orbit of CHAMP (top) and GOCE (bottom) in April 2010. The C/DA is applied using CHAMP data as observation, then the C/DA-NRLMSISE-00 densities in the forecast mode are shown in both plots.

Table 3.9: A summary of the statistical measures derived for the original NRLMSISE-00, JB08, HASDM, and C/DA-NRLMSISE-00 compared to the TNDs derived from the GOCE measurements in April 2010.

Model	RMSE (kg/m^3)	Bias (kg/m^3)	coefficient of efficiency	Correlation	AAPD (%)	RE(%)
NRLMSISE-00	5.77×10^{-12}	2.90×10^{-12}	0.14	0.63	18.60	46.25
JB08	5.40×10^{-12}	2.01×10^{-12}	0.24	0.64	17.42	43.32
HASDM	8.35×10^{-12}	6.51×10^{-12}	-0.80	0.58	27.59	65.51
C/DA-NRLMSISE-00	4.29×10^{-12}	-6.77×10^{-13}	0.52	0.71	12.72	34.41

ing EOFs and PCs are depicted in figure 3.17. Similar to the previous sections, PCA is also applied on the TND differences (of the original NRLMSISE-00 and the C/D-NRLMSISE-00 in the forecasting mode) to better emphasise relative differences. The first mode (EOF1 and PC1 in figure 3.17) shows the response of TND changes to the storm condition, where the original and C/DA model indicates a sharp sudden change on April 5^{th} due to changes in the K_p index.

The second mode (EOF2 and PC2 in figure 3.17) represents the diurnal changes. The maximum magnitude of the first and second mode derived from C/DA model reach up to $1.6 \times 10^{-10} kg^{m3}$ and $1.2 \times 10^{-10} kg^{m3}$, respectively.

Figure 3.18 presents the average and the standard deviations of spatial differences

between the original NRLMSISE-00 and C/DA-NRLMSISE-00, where the average and maximum value of differences (an indication of biases) are found to be $1.4 \times 10^{-11} kg^{m3}$ and $2.1 \times 10^{-11} kg^{m3}$. The first mode of the PCA of differences indicates disagreements between models in both detecting the storm effect on TND changes within the after-storm phase until it is settled. This difference reaches to $2.7 \times 10^{-11} kg^{m3}$ during the storm on April 5^{th}, 2010. The second mode of differences mainly indicates their diurnal mismatch with the minimum and maximum magnitude of $-9.7 \times 10^{-12} kg^{m3}$ and $1.2 \times 10^{-11} kg^{m3}$, respectively.

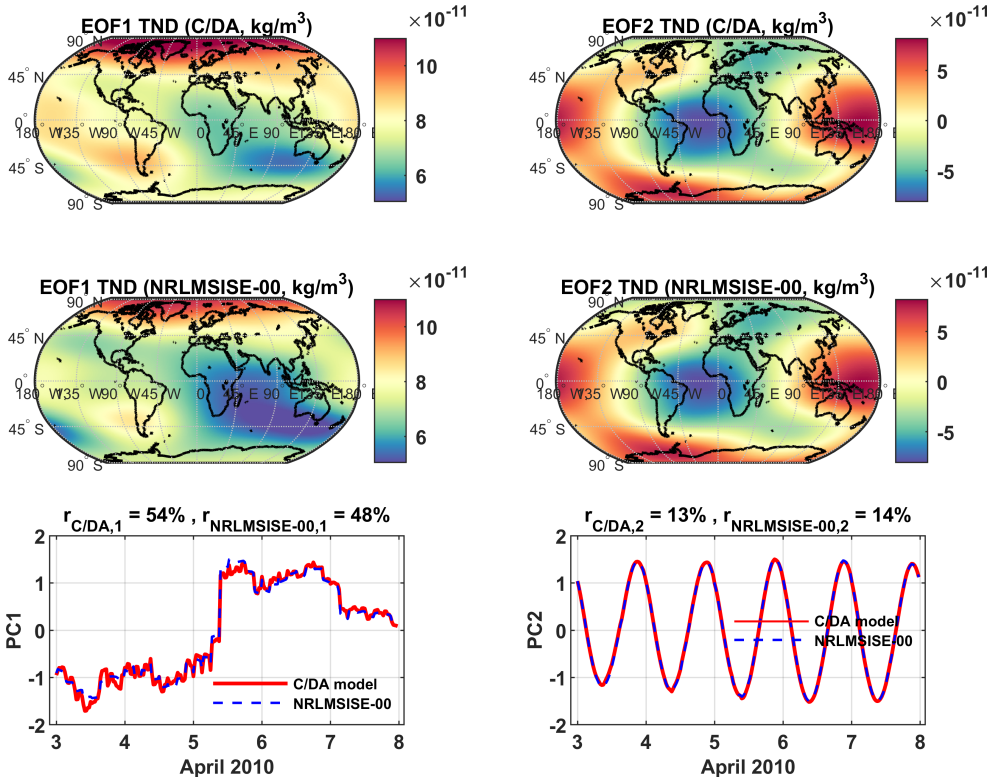

Figure 3.17: An overview of the PCA results applied on the TND estimates of the original NRLMSISE-00 and those of C/DA-NRLMSISE-00 at 150 km during Storm4 in April 2010. The anomaly maps (EOFs) are in terms of kg/m^3, which can be multiplied by the unit less time series (PCs) on the bottom to derive the PCA's orthogonal modes. The first mode represents 48% and 54%, and the second mode indicates 14% and 13% of the total variance of the original and C/DA models, respectively.

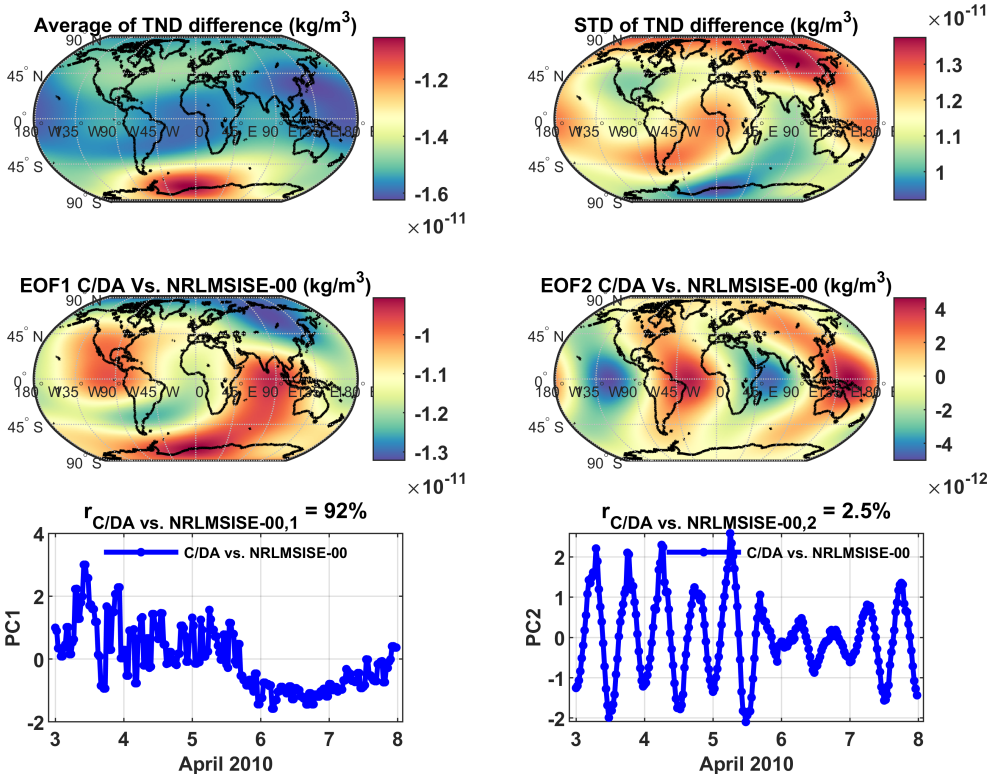

Figure 3.18: An overview of the PCA results derived from the TND differences of the original NRLMSISE-00 and C/DA-NRLMSISE-00 at 150 km during Storm4 in April 2010. The first mode represents 92% of the total variance of TND differences and the second mode indicates 2.5% of it.

3.4.5 Evaluation of Storm5, March 2015

Storm5 during March 2015 corresponds to one of the most considerable geomagnetic activity within the 24^{th} solar cycle ([43]). The variation of the geomagnetic index K_p during this period is shown in figure (3.1,e). In this experiment, we used the TNDs of Swarm-C during March 15^{th}-26^{th}, 2015 as assimilation observation. Then those of Swarm-C and Swarm-B are applied for validating the model forecasts.

Similar to other storms, the C/DA outputs are generated for the hourly forecasts. The along track TND results are represented in figure 3.19. In addition, Table 3.10 and Table 3.11 summarise various statistical measures during this storm along Swarm-C and Swarm-B, respectively. They show the overall best of the C/DA to the space-based TND estimation, for example, the correlation coefficients between TNDs of the original NRLMSISE-00 / JB08 / HASDM / C/DA-NRLMSISE-00 and those of Swarm-C (Swarm-B) are found to be 120(148), 87(105), 75(80), and 96(97)%.

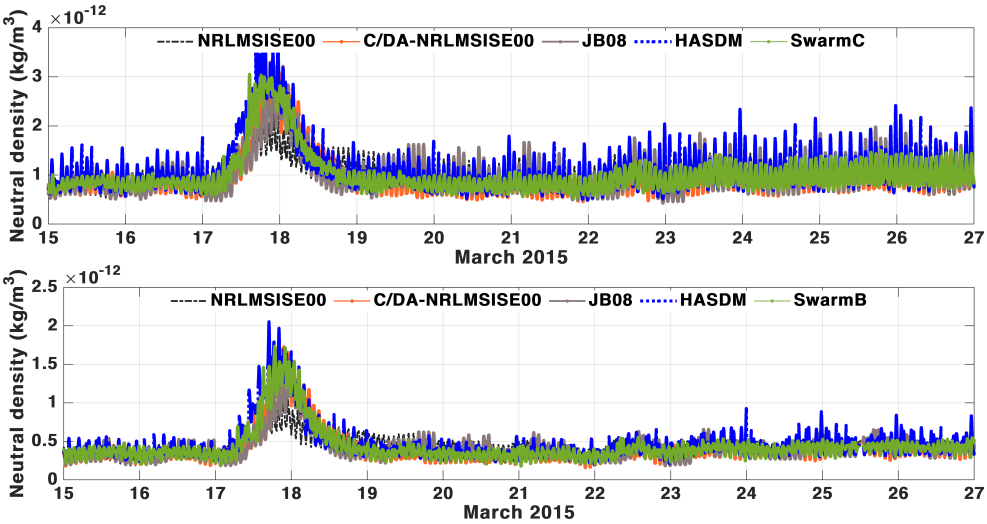

Figure 3.19: A comparison of the time series of TNDs derived from the original NRLMSISE-00, JB08, HASDM, and C/DA-NRLMSISE-00 along the orbits of Swarm-C (top) and the Swarm-B (bottom) during Storm5 in March 2015. Here, the TNDs along Swarm-C are used for implementing the C/DA.

Here, we skip presenting the PCA results of the global TND fields because they do not add more insights than the investigations in the previous sections. From our experiments, we detected that the C/DA can change the TND estimates globally, and this impact can be felt in all vertical altitudes. We also observed that, as expected, those C/DA TNDs corresponding to the altitudes of Swarm-B and Swarm-C are very

Table 3.10: A summary of statistical measures between the original NRLMSISE-00, JB08, HASDM, and C/DA-NRLMSISE-00 compared to the TNDs derived from Swarm-C during Storm5 in March 2015.

Model	RMSE (kg/m^3)	Bias (kg/m^3)	Coefficient Of Efficiency	Correlation	AAPD (%)	RE(%)
NRLMSISE-00	2.72×10^{-13}	3.66×10^{-14}	0.57	1.20	16.40	50.58
JB08	2.44×10^{-13}	7.13×10^{-15}	0.65	0.87	16.47	45.39
HASDM	2.52×10^{-13}	1.20×10^{-13}	0.63	0.75	16.86	45.85
C/DA-NRLMSISE-00	1.44×10^{-13}	-1.26×10^{-14}	0.88	0.96	8.61	26.82

Table 3.11: A summary of statistical measures between the original NRLMSISE-00, JB08, HASDM, and C/DA-NRLMSISE-00 compared to the TNDs derived from Swarm-B during Storm5 in March 2015.

Model	RMSE (kg/m^3)	Bias (kg/m^3)	coefficient of efficiency	Correlation	AAPD (%)	RE(%)
NRLMSISE-00	1.41×10^{-13}	3.02×10^{-15}	0.57	1.48	18.02	60.95
JB08	1.19×10^{-13}	-1.86×10^{-14}	0.69	1.05	18.54	51.55
HASDM	1.15×10^{-13}	3.66×10^{-14}	0.71	0.80	20.08	48.81
C/DA-NRLMSISE-00	7.48×10^{-14}	-1.61×10^{-14}	0.87	0.97	10.46	32.31

close to the observations.

3.4.6 Evaluation of Storm 6, September 2017

A considerable geomagnetic storm happened on September 2017. Variations of the geomagnetic index K_p (figure (3.1,f)) indicate that the period of September 6^{th}-9^{th} contains the event, and therefore, it is chosen as Storm6. The TND estimates of Swarm-C are chosen for performing the C/DA, and those of Swarm-C and Swarm-B are used for validation. The setup of the assessment is implemented in the same manner as the along track assessments of the previous sections. The numerical results are summarised in Table 3.12 and Table 3.13 representing the statistical measures along Swarm-C and Swarm-B, respectively. In all cases, we observed a better fit of C/DA-NRLMSISE-00 to the space-based TND estimates. The global impact of the C/DA on estimating TNDs is confirmed by performing the PCA technique, but the results are skipped here to keep the length of the report short.

Table 3.12: A summary of the statistical measures derived from the original NRLMSISE-00, JB08, HASDM, and C/DA-NRLMSISE-00 compared to the TNDs of Swarm-C during Storm6 in September.

Model	RMSE (kg/m^3)	Bias (kg/m^3)	Coefficient Of Efficiency	Correlation	AAPD (%)	RE(%)
NRLMSISE-00	2.88×10^{-13}	2.46×10^{-13}	0.07	0.78	54.16	54.60
JB08	1.57×10^{-13}	-3.98×10^{-14}	0.72	0.87	19.17	29.85
HASDM	1.73×10^{-13}	5.86×10^{-14}	0.66	0.74	21.28	32.33
C/DA-NRLMSISE-00	1.26×10^{-13}	-1.52×10^{-14}	0.82	0.96	16.19	23.82

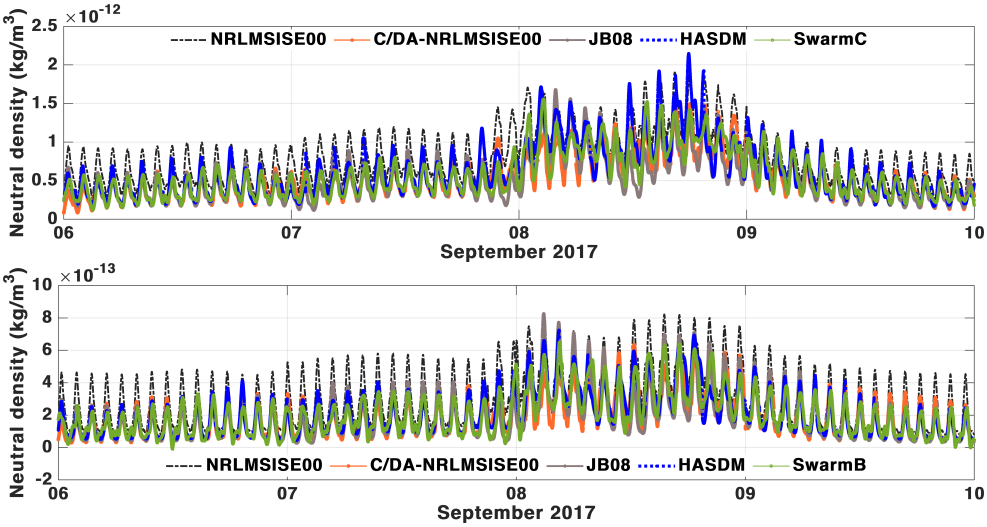

Figure 3.20: A comparison of the along track TND estimates derived from the NRLMSISE-00, JB08, HASDM, and those of the C/DA-NRLMSISE-00 model in the forecasting mode along Swarm-C (top) and Swarm-B (bottom). These results correspond to Storm6 in September 2017.

Table 3.13: A summary of the statistical measures derived from the original NRLMSISE-00, JB08, HASDM, and C/DA-NRLMSISE-00 compared to the TNDs of Swarm-B during Storm6 in September.

Model	RMSE (kg/m^3)	Bias (kg/m^3)	coefficient of efficiency	Correlation	AAPD (%)	RE(%)
NRLMSISE-00	1.27×10^{-13}	1.01×10^{-13}	0.07	0.68	147.18	67.83
JB08	6.58×10^{-14}	-1.13×10^{-14}	0.75	0.81	65.02	34.96
HASDM	6.09×10^{-14}	9.41×10^{-15}	0.78	0.85	76.74	32.16
C/DA-NRLMSISE-00	5.78×10^{-14}	-3.99×10^{-15}	0.80	0.91	70.63	30.76

3.4.7 Evaluation of Storm7, September 2020

The period of September 23^{th}-29^{th}, 2020 is chosen as Storm7. Variations of K_p are shown in figure (3.1,g), for which the geomagnetic activity is found not to be extremely high (maximum 4), but it is relatively higher than the rest of the month. The TND estimates along Swarm-C are used as observation of the C/DA experiment. Then, those of Swarm-C and Swarm-B are used for validation.

Figure 3.21 displays the along track time-series of TNDs derived from models and observations during 23^{th}-29^{th}. Both empirical models JB08 and the original NRLMSISE-00 over-estimate (by scale ~ 2) the TND evolution during this period. However, the numerical results indicate that this problem has considerably decreased after implementing the C/DA. It is worth mentioning here that we did not perform a

comparison with the HASDM model outputs during Storm7 because the open-access results of this model after 2019 are not available. Table 3.14 and Table 3.15 summarise the validation results against Swarm-C and Swarm-B, respectively.

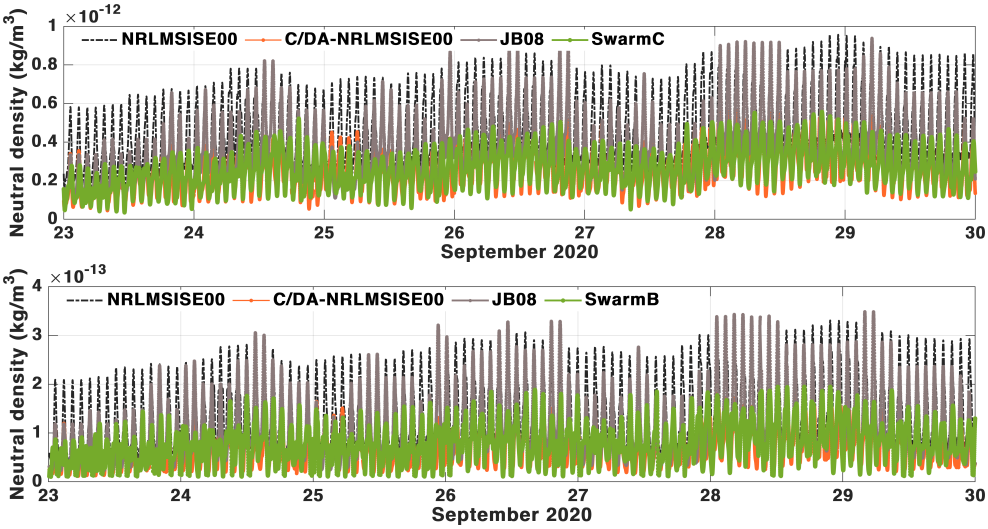

Figure 3.21: A comparison of the along track TND estimates derived from the original NRLMSISE-00, JB08, and C/DA-NRLMSISE-00 models along the Swarm-C (top) and Swarm-B (bottom) orbits during Storm7 in September 2020.

Table 3.14: A summary of the statistical measures between the original NRLMSISE-00, JB08, and C/DA-NRLMSISE-00 compared to the TNDs derived from Swarm-C during Storm 7 in September 2020.

Model	RMSE (kg/m^3)	Bias (kg/m^3)	Coefficient Of Efficiency	Correlation	AAPD (%)	RE(%)
NRLMSISE-00	2.45×10^{-13}	2.16×10^{-13}	-4.43	0.46	91.09	131.28
JB08	1.53×10^{-13}	1.06×10^{-13}	-1.13	0.47	48.48	82.36
C/DA-NRLMSISE-00	0.71×10^{-13}	-3.75×10^{-15}	0.54	0.71	21.35	37.88

Table 3.15: A summary of the statistical measures between the original NRLMSISE-00, JB08, and C/DA-NRLMSISE-00 compared to the TNDs derived from Swarm-B during Storm7 in September 2020.

Model	RMSE (kg/m^3)	Bias (kg/m^3)	coefficient of efficiency	Correlation	AAPD (%)	RE(%)
NRLMSISE-00	8.36×10^{-14}	6.58×10^{-14}	-3.29	0.40	110.29	141.23
JB08	5.97×10^{-14}	3.16×10^{-14}	-1.18	0.41	67.15	100.86
C/DA-NRLMSISE-00	3.05×10^{-14}	-8.50×10^{-15}	0.42	0.73	39.40	51.52

To illustrate what could be expected as a global impact of integrating space-based TNDs with NRLMSISE-00 during a period with moderate geomagnetic activity, PCA is applied. For this, the TND estimates of the original and calibrated NRLMSISE-00 model are considered globally with 30 minutes temporal sampling at 350 km altitude. Here we only show the results of the PCA of differences between these models in figure 3.22. The global differences between the average TND fields indicate that in this altitude, one might expect a bias of the magnitude of $\sim 10^{-12} kg^{m3}$ (see the plot on top-left). The standard deviations of differences are found to be at the order of $\sim 10^{-13} kg^{m3}$, which is important for representing the temporal fluctuations (see the plot on top-right). The average magnitude of the first two modes of the differences is found to be around $10^{-13} kg^{m3}$, where the first mode (EOF1 and PC1) indicates a mixture of the diurnal/semi-diurnal differences, and a jump due to the geomagnetic changes on September 25^{th}-26^{th} (see the plots on middle- and bottom-left). The second mode (EOF2 and PC2) is dominated by the out of phase diurnal differences between the two models (see the plots on the middle- and bottom-right).

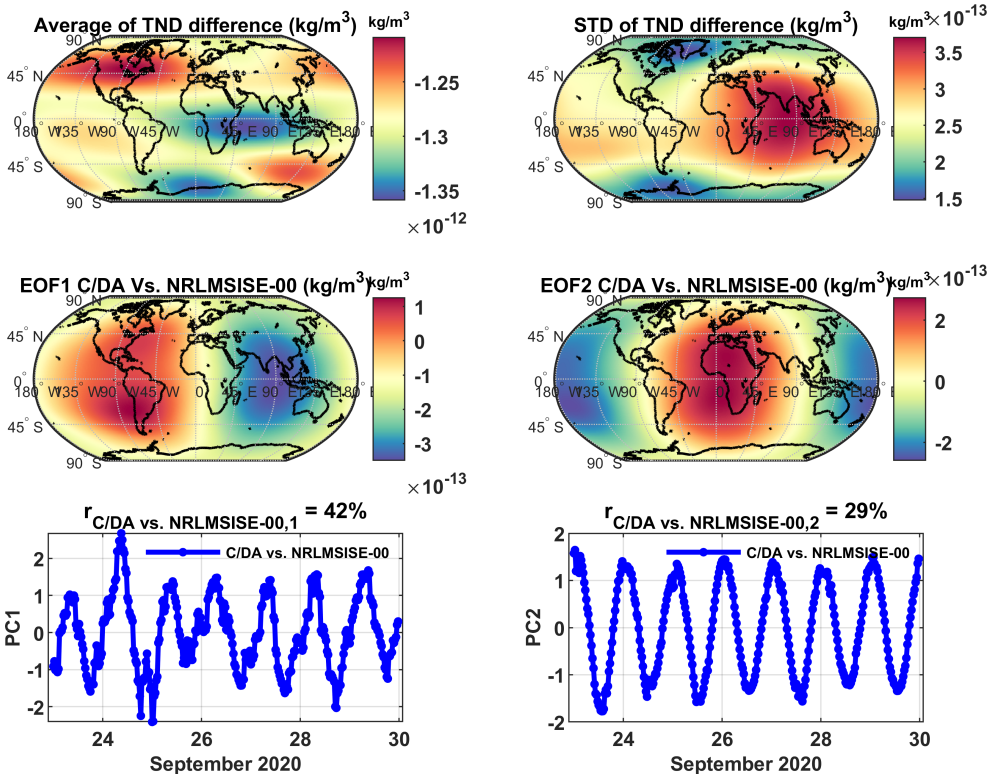

Figure 3.22: An overview of the PCA results derived from the global TND differences between the original NRLMSISE-00 and C/DA-NRLMSISE-00 at 350 km during Storm7 in September 2020. The anomaly maps (EOFs) are in terms of kg/m^3, which can be multiplied by the unit less time series (PCs) on the right to derive orthogonal modes. The first mode of differences represents 42% of the total variance of TND differences and the second mode indicates 29% of the variance.

CHAPTER 4

Conclusion

In this report, we investigated the possibility of applying the publicly available space-based along track Thermosphere Neutral Density (TND) data for producing a global multi-level TND data set (a new level 3, L3, TND product). Unlike other available global data assimilation outputs, the proposed L3 data product is based purely on openly available data, which makes it reproducible. Besides, CHAMP, Swarm, GRACE, and GRACE-FO measurements provide the opportunity to produce high resolution and continuous global TND estimates.

To achieve a comprehensive assessment, seven periods between 2003-2020 with considerable geomagnetic activity are considered (the periods are labeled Storm1 to Storm7 in the previous chapter, see figure 3.1). During these events, various combinations of the space-based TND estimates are investigated to produce the new L3 products. The validations are performed in the (one-hour) forecast phase with the space-based data that were not used for our production. The study has tested the observations of CHAMP, GRACE and Swarm to be used for producing the L3 TND products and those of CHAMP, GRACE, GOCE, and Swarm are applied for validation, see Table 3.1.

These experiences are performed by considering the NRLMSISE-00 model ([25]) as the basis and the simultaneous Calibration and Data Assimilation (C/DA, [10, 12]) is applied to fit the original modelled TND outputs to those of the space-based estimates. Therefore, the new model is named C/DA-NRLMSISE-00, which can be used to simulate TNDs and individual neutral components globally on various altitudes, therefore, it can also be used for producing a new set of L3 TND data product. The updated model might be useful for applications such as orbit determination and space weather. To produce the end-user L3 TND data, meaningful spatial and temporal sampling and the vertical sensitivity are also investigated. In what follows, the featured conclusions are summarised.

1- Producing the C/DA model (needed for estimating the L3 products) is a sequential optimisation procedure, which depends on the quality of space-based observations and the quality of the basis model to simulate the dynamic of physical processes that drive TND changes. Therefore, it is extremely difficult to define a theoretical period (time-window) to achieve the best fit between the basis model and measurements, and at the same time, to guarantee an acceptable forecasting ability. This is because models cannot reproduce the physical processes and the quality of the measurements and the input indices can change in

space and time. Our investigations during the seven relatively high K_p periods indicate that an assimilation window of up to to 4 hours is realistic to perform a successful C/DA, whose forecasting results are close to the assessed space-based TND measurements. Selecting longer assimilation windows will have negative impacts on the fitting-related statistical measures, thus it is not recommended, see Section 3.2 and figure 3.2.

2- The choice of spatial (horizontal and vertical) and temporal sampling is investigated in Section 3.3 by implementing empirical covariance matrices. The results indicate that the time interval of 45 minutes to one hour, the horizontal sampling of five degrees, and the vertical sampling of 25 km can be realistic for producing the final global L3 TND fields. This investigation is however limited to the selection of the NRLMSISE-00 as the basis model and the few periods that are covered in this report. A more comprehensive assessment might provided alternative suggestions. Besides, our recommendation does not take into the account the end-user requirements and neither the data storage capacity, as well as download and upload requirements for sharing long-term L3 data.

3- The global investigations of the TND estimates, e.g., drawn by applying PCA in Section 3.4, indicate that even though the vertical coverage of space-based measurements is limited, C/DA can extend their impact to various levels. Our investigations indicate that the range of impact is the same as the vertical coverage of the basis model, i.e., NRLMSISE-00. However, our validation is limited by the data availability. For example, we could test the minimum altitude of around 270 km using GOCE during Storm4 in 2010 and the maximum altitude of around 540 km using Swarm data in Storm5, 6, and 7.

4- The dominant changes in the TND estimates derived from the PCA, as well as computing the biases between the original and C/DA-NRLMSISE-00 are found to be considerably big for many geodetic applications. Other available models such JB08 and HASDM also indicate biases, where that of JB08 is found to be similar to the original NRLMSISE-00, but much smaller values are found for HASDM. During Storm4 in 2010, HASDM indicates considerable bias of $\sim 10^{-12}$ kg/m^3 at the altitude of GOCE, i.e., $\sim$ 270 km. Generally speaking, a magnitude of bias around $1 - 4 \times 10^{-12}$ kg/m^3 at the altitude of $\sim$ 300-400 km can be found from most of the available models, which will be considerably decreased by producing the proposed L3 data.

The global and along track TND data sets during the seven storm periods of this study are submitted along with this report to the Swarm DISC team. These data sets can be used for further investigations and validations.

Bibliography

[1] A Albertella, F Migliaccio, and F Sanso. "GOCE: The Earth gravity field by space gradiometry." In: *Modern celestial mechanics: from theory to applications*. Springer, 2002, pp. 1–15. DOI: 10.1023/A:1020104624752.

[2] B Bowman et al. "A new empirical thermospheric density model JB2008 using new solar and geomagnetic indices." In: *AIAA/AAS Astrodynamics Specialist Conference and Exhibit*. 2008, p. 6438. DOI: 10.2514/6.2008-6438.

[3] SM Codrescu, MV Codrescu, and M Fedrizzi. "An ensemble Kalman filter for the thermosphere-ionosphere." In: *Space Weather* 16.1 (2018), pp. 57–68. DOI: 10.1002/2017SW001752.

[4] E Doornbos. *Thermospheric density and wind determination from satellite dynamics*. Springer Science & Business Media, 2012. DOI: http://resolver.tudelft.nl/uuid:33002be1-1498-4bec-a440-4c90ec149aea.

[5] E Doornbos, H Klinkrad, and PNAM Visser. "Atmospheric density calibration using satellite drag observations." In: *Advances in Space Research* 36.3 (2005), pp. 515–521. DOI: 10.1016/j.asr.2005.02.009.

[6] E Doornbos, H Klinkrad, and PNAM Visser. "Use of two-line element data for thermosphere neutral density model calibration." In: *Advances in Space Research* 41.7 (2008), pp. 1115–1122. DOI: 10.1016/j.asr.2006.12.025.

[7] G Evensen. "The ensemble Kalman filter for combined state and parameter estimation." In: *IEEE Control Systems Magazine* 29.3 (2009), pp. 83–104. DOI: 10.1109/MCS.2009.932223.

[8] F Flechtner et al. "Status of the GRACE follow-on mission." In: *Gravity, geoid and height systems*. Vol. 141. Springer, 2014, pp. 117–121. DOI: 10.1007/978-3-319-10837-7_15.

[9] E Forootan. "Statistical signal decomposition techniques for analyzing time-variable satellite gravimetry data." PhD thesis. University of Bonn, 2014. URL: https://hdl.handle.net/20.500.11811/1452.

[10] E Forootan et al. "A simultaneous calibration and data assimilation (C/DA) to improve NRLMSISE00 using thermospheric neutral density (TND) from space-borne accelerometer measurements." In: *Geophysical Journal International* 224.2 (Oct. 2020), pp. 1096–1115. DOI: 10.1093/gji/ggaa507.

[11] E Forootan et al. “Estimating and predicting corrections for empirical thermospheric models.” In: *Geophysical Journal International* 218.1 (2019), pp. 479–493. DOI: 10.1093/gji/ggz163.

[12] E Forootan et al. “Forecasting global and multi-level thermospheric neutral density and ionospheric electron content by tuning models against satellite-based accelerometer measurements.” In: *Scientific Reports* 12.1 (2022), pp. 1–19. DOI: 10.1038/s41598-022-05952-y.

[13] HC Godinez et al. “Specification of the ionosphere-thermosphere using the ensemble Kalman filter.” In: *International Conference on Dynamic Data-Driven Environmental Systems Science*. Springer. 2014, pp. 274–283. DOI: 10.1007/978-3-319-25138-7_25.

[14] RE Kalman. “A new approach to linear filtering and prediction problems.” In: *Journal of Basic Engineering* 82.1 (1960), pp. 35–45. DOI: 10.1115/1.3662552.

[15] S Krauss, M Temmer, and S Vennerstrom. “Multiple satellite analysis of the Earth’s thermosphere and interplanetary magnetic field variations due to ICME/-CIR events during 2003–2015.” In: *Journal of Geophysical Research: Space Physics* 123.10 (2018), pp. 8884–8894. DOI: 10.1029/2018JA025778.

[16] T Matsuo. “Upper atmosphere data assimilation with an ensemble Kalman filter.” In: *Modeling the ionosphere-thermosphere system (eds J. Huba, R. Schunk and G. Khazanov)* (2014), pp. 273–282. DOI: 10.1002/9781118704417.ch22.

[17] T Matsuo and JM Forbes. “Principal modes of thermospheric density variability: Empirical orthogonal function analysis of CHAMP 2001-2008 data.” In: *Journal of Geophysical Research: Space Physics* 115 (2010), A07309. DOI: 10.1029/2009JA015109.

[18] T Matsuo, AD Richmond, and G Lu. “Optimal interpolation analysis of high-latitude ionospheric electrodynamics using empirical orthogonal functions: estimation of dominant modes of variability and temporal scales of large-scale electric fields.” In: *Journal of Geophysical Research: Space Physics* 110 (2005), A06301. DOI: 10.1029/2004JA010531.

[19] T Matsuo, AD Richmond, and DW Nychka. “Modes of high-latitude electric field variability derived from DE-2 measurements: Empirical Orthogonal Function (EOF) analysis.” In: *Geophysical Research Letters* 29.7 (2002). DOI: 10.1029/2001GL014077.

[20] PM Mehta and R Linares. “A new transformative framework for data assimilation and calibration of physical ionosphere-thermosphere models.” In: *Space Weather* 16 (2018), pp. 1086–1100. DOI: 10.1029/2018SW001875.

[21] PM Mehta, R Linares, and EK Sutton. “Data-driven inference of thermosphere composition during solar minimum conditions.” In: *Space Weather* 17.9 (2019), pp. 1364–1379. DOI: 10.1029/2019SW002264.

[22] PM Mehta et al. “New density estimates derived using accelerometers on board the CHAMP and GRACE satellites.” In: *Space Weather* 15.4 (2017), pp. 558–576. DOI: 10.1002/2016SW001562.

[23] AV Morozov et al. “Data assimilation and driver estimation for the Global ionosphere–thermosphere model using the ensemble adjustment Kalman filter.” In: *Journal of Atmospheric and Solar-Terrestrial Physics* 104 (2013), pp. 126–136. DOI: 10.1016/j.jastp.2013.08.016.

[24] D Pérez et al. “Orbit-centered atmospheric density prediction using artificial neural networks.” In: *Acta Astronautica* 98 (2014), pp. 9–23. DOI: 10.1016/j.actaastro.2014.01.007.

[25] JM Picone et al. “NRLMSISE-00 empirical model of the atmosphere: statistical comparisons and scientific issues.” In: *Journal of Geophysical Research: Space Physics* 107.A12 (2002), p. 1468. DOI: 10.1029/2002JA009430.

[26] MD Pilinski et al. “Improved orbit determination and forecasts with an assimilative tool for satellite drag specification.” In: *Advanced Maui Optical and Space Surveillance Technologies Conference*. Vol. 104. 2016. DOI: 2016amos.confE.104P.

[27] R Preisendorfer. *Principal component analysis in meteorology and oceanography*. Elsevier, 1988.

[28] L Qian and SC Solomon. “Thermospheric density: an overview of temporal and spatial variations.” In: *Space Science Reviews* 168.1 (2012), pp. 147–173. DOI: 10.1007/s11214-011-9810-z.

[29] L Qian et al. “Solar flare impacts on ionospheric electrodyamics.” In: *Geophysical Research Letters* 39.6 (2012). DOI: 10.1029/2012GL051102.

[30] C Reigber, H Lühr, and P Schwintzer. “CHAMP mission status.” In: *Advances in Space Research* 30.2 (2002), pp. 129–134. DOI: 10.1016/S0273-1177(02)00276-4.

[31] Haibing Ruan et al. “An Exospheric Temperature Model Based On CHAMP Observations and TIEGCM Simulations.” In: *Space Weather* 16.2 (2018), pp. 147–156. DOI: 10.1002/2017SW001759.

[32] M Schumacher. “Methods for assimilating remotely-sensed water storage changes into hydrological models.” PhD thesis. University of Bonn, 2016. URL: http://hss.ulb.uni-bonn.de/2016/4508/4508.htm.

[33] C Shi et al. “Calibrating the scale of the NRLMSISE00 model during solar maximum using the two line elements dataset.” In: *Advances in Space Research* 56.1 (2015), pp. 1–9. DOI: 10.1016/j.asr.2015.03.024.

[34] JS Shim et al. “Systematic evaluation of ionosphere/thermosphere (IT) models.” In: *Modeling the ionosphere–thermosphere system*. American Geophysical Union (AGU), 2014. Chap. 13, pp. 145–160. ISBN: 9781118704417. DOI: 10.1002/9781118704417.ch13.

[35] SC Solomon et al. “Causes of low thermospheric density during the 2007–2009 solar minimum.” In: *Journal of Geophysical Research: Space Physics* 116.A2 (2011). DOI: 10.1029/2011JA016508.

[36] MF Storz et al. “High accuracy satellite drag model (HASDM).” In: *Advances in Space Research* 36.12 (2005). Space Weather, pp. 2497–2505. DOI: 10.1016/j.asr.2004.02.020.

[37] EK Sutton, RS Nerem, and JM Forbes. “Density and winds in the thermosphere deduced from accelerometer data.” In: *Journal of Spacecraft and Rockets* 44.6 (2007), pp. 1210–1219. DOI: 10.2514/1.28641.

[38] BD Tapley et al. “GRACE measurements of mass variability in the Earth system.” In: *Science* 305.5683 (2004), pp. 503–505. DOI: 10.1126/science.1099192.

[39] DA Vallado and D Finkleman. “A critical assessment of satellite drag and atmospheric density modeling.” In: *Acta Astronautica* 95 (2014), pp. 141–165. ISSN: 0094-5765. DOI: 10.1016/j.actaastro.2013.10.005.

[40] K Vielberg et al. *TND-IGG RL01: Thermospheric neutral density from accelerometer measurements of GRACE, CHAMP and Swarm*. data set. 2021. DOI: 10.1594/PANGAEA.931347.

[41] PNAM Visser et al. “Thermospheric density and wind retrieval from Swarm observations.” In: *Earth, Planets and Space* 65.11 (2013), pp. 1319–1331. DOI: 10.5047/eps.2013.08.003.

[42] L Weng et al. “An exospheric temperature model from CHAMP thermospheric density.” In: *Space Weather* 15.2 (2017), pp. 343–351. DOI: 10.1002/2016SW001577.

[43] C-C Wu et al. “The first super geomagnetic storm of solar cycle 24:“The St. Patrick’s day event (17 March 2015)”.” In: *Earth, Planets and Space* 68.1 (2016), pp. 1–12. DOI: 10.1186/s40623-016-0525-y.